# Imaging the Breakdown of the Blood-Brain Barrier in Mice with Modeled Alzheimer's Disease

A thesis submitted in partial fulfillment of the requirements for the degree of Bachelor of Science with Honors in the Neuroscience concentration of Brown University

Joseph Namkung

Class of 2023

Dr. Jonghwan Lee

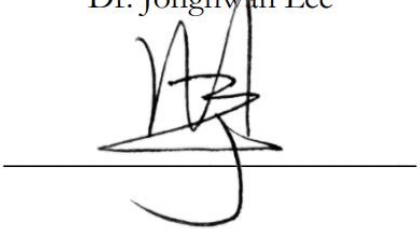

Submitted on

April 21st, 2023

**Acknowledgements**

I would first like to thank Dr. Jonghwan Lee, my PI and thesis advisor, for the opportunity to work in his lab and for his guidance on the experimental design of this project. Thank you for all your assistance over these past two years and for your continued flexibility, patience, and encouragement despite the roadblocks and challenges we faced.

I owe a tremendous amount of gratitude to Sinda Fekir, who mentored me on almost every aspect of this project, from perfusion training to recommendations for software to analyze imaged slices. Her assistance with tail vein injections of Evans Blue dye proved vital for completing this project in a reasonable timeframe, and her patient, honest advice and extensive knowledge were invaluable to my development as a scientist and researcher.

I would also like to thank Jang-hoon Lee and Jiarui Nie for taking the time to answer my questions and show me the ropes in lab. I especially owe Jang-hoon a lot of thanks for procuring the materials and equipment I requested over the course of the project. I owe thanks to Leduc Bioimaging Facility and to Geoff Williams and Jacqueline Ecolastico for imaging my slides and for their detailed advice.

I would like to thank my parents, Chan and Sabrina, and my friends for their support and faith in me. I would especially like to thank David Moon and Ryan Lum for patiently listening to all my stories about lab and Kevin Nguyen for his solidarity and support as a fellow neuroscience honors candidate. I would also like to thank God for the many people who have helped me throughout this journey and for the opportunities provided me. Last, but certainly not least, I would like to thank the mice who gave their lives for this project.

## Table of Contents

**Abstract**

The blood-brain barrier (BBB) has been recently identified as a key factor involved in the origin and pathological progression of Alzheimer's disease (AD). The BBB normally plays a role in carefully maintaining the homeostasis of the neural environment by establishing a highly selectively permeable barrier between the CNS and the peripheral microvasculature. Dysfunction of the BBB, also called BBB breakdown, results in altered, usually increased permeability and is a potential early biomarker of AD and cognitive dysfunction. BBB breakdown is either initiated or accelerated by the ε4 variant of the *apolipoprotein E* (*APOE*) gene, also known as ApoE4. ApoE4 may impact the BBB through multiple processes including degradation of pericytes, aberrant transport of clotting factors and the key AD biomarker amyloid-β, and disruption of BBB transport mechanisms. This thesis further investigates the degeneration of the BBB in relation to AD using an Evans Blue (EB) dye assay in ApoE4 mice compared with ApoE3 and wild-type (WT) controls. Fluorescent EB dye binds to the macromolecule albumin, which is too large to cross through the highly selective BBB. However, BBB breakdown decreases this selectivity and increases permeability, allowing EB to enter the brain. Intensity of EB dye within brain slices was taken as a measure of BBB permeability. This thesis analyzes the pattern of staining within ApoE4, ApoE3, and WT brains and statistically analyzes the intensity of EB staining across genotype, brain region, and sex groups. We observed concentrated staining in the cortex and hippocampus, as well as the substantia nigra pars reticulata. We found that ApoE4 mice brains contain significantly more BBB disruption than ApoE3 and WT brains. Our findings provide additional insights into the pattern of AD pathology within the brain and confirm that ApoE4 contributes to the degradation of the BBB.

## Introduction

### *Alzheimer's Disease*

Alzheimer's disease (AD) is a debilitating neurodegenerative disease that causes progressively increasing cognitive decline. The symptomology of AD primarily involves impaired memory and memory consolidation, speech and language impairment, confusion, and executive dysfunction, including changes in personality. Like many other neurodegenerative disorders, AD is circuit-selective, affecting the neocortex, especially the frontal lobe, hippocampus, and entorhinal cortex. As neurons degenerate and die, the ventricles dilate, and dilated lateral ventricles are commonly seen in AD. As the most common neurodegenerative disease and cause of dementia, it affects around 6.7 million Americans and 55 million people worldwide (Alzheimer's Association, 2023; Gauthier et al., 2022). These numbers are expected to increase drastically as the world's population grows older: the number of Americans with AD is expected to double by 2050, and worldwide estimates predict 139 million people with AD by 2050 (Alzheimer's Association, 2023; Gauthier et al., 2022). As a result, Alzheimer's Disease is one of the most pressing global public health concerns, but despite its danger and the extensive research done on the topic, much has yet to be understood about Alzheimer's, particularly its origins.

### *Hypothesized Causes and Contributing Factors to AD*

Numerous factors contribute to AD and increase the risk of having AD, the foremost of these being age. The age of onset is estimated to be around 65 years old, and the frequency of onset doubles every 5 years after age 60 (Scheltens et al., 2021; Cummings, 2008). Alzheimer's also has a strong genetic component, with the strongest risk gene being *APOE ε4* (sometimes written as ApoE4). The *APOE* gene encodes for apolipoprotein E (ApoE), which is involved in transport of cholesterol and other fats in the bloodstream. ApoE also binds Aβ, a critically important biomarker

for AD. Three main variants of *APOE* exist. *ε4* increases the risk of AD, and while carrying one copy is sufficient for inducing risk, having two copies increases this risk further (National Institute on Aging, 2023). The increase in AD risk caused by ApoE4 may be caused by aberrant transport of Aβ (Hultman et al., 2013). *ε3* is theorized to have no effect on the risk of AD and is thus frequently used as a control group. The *ε2* variant seems to serve a protective role and although it does not eliminate the possibility of AD, it halves the risk of AD over a person's lifetime (Scheltens et al., 2021). Additionally, if AD occurs in people with *APOE ε2*, it often has a delayed onset (National Institute on Aging, 2023). The *APP* gene that encodes for amyloid precursor protein (APP) is also considered as a possible contributor, as are two genes that encode for proteins involved in its processing, presenilin-2 (*PSEN2*) and presenilin-1 (*PSEN1*). However, these genes are not requirements for AD. Women have a greater risk of AD as well, although this link has not been fully explored. Cardiovascular health is another contributing factor, and poor heart health can increase the risk of dementia and AD (Scheltens et al., 2021). Conversely, regular exercise, good sleeping habits and stress management, and, curiously, a healthy gut microbiome seem to act as protective factors against the risk of AD (Segarra et al., 2020).

AD pathogenesis is notoriously hard to understand because of the complexity of the systems involved, such as memory and personality. Many hypotheses for the etiology of Alzheimer's exist, and most focus on two key biomarkers: amyloid-beta (Aβ) and phosphorylated tau proteins (p-tau). The most known of these is the amyloid-cascade hypothesis. This hypothesis draws on the observed presence of Aβ aggregations, called plaques, in AD brains after autopsy. The cascade theory posits that Aβ, formed from amyloid precursor protein, is ultimately responsible for AD pathology, from the neurofibrillary tangles (NFTs) also characteristic of the disease to neuron death and dementia symptoms (Hardy & Higgins, 1992). APP has two options for processing by enzymes, one of which leads to Aβ. Aβ then aggregates, leading to neurotoxicity. This processing is influenced by the

*PSEN1* and *PSEN2* genes mentioned previously. This cascade was considered to be a causal, linear process, and showed promise as a theory of AD pathogenesis. Aβ plaques are always found in patients with Alzheimer's and are toxic to neurons in culture, which lends strength to it as a cause of AD. However, these plaques can be and are found at significant levels in cognitively normal, non-AD patients (Herrup, 2015). Therefore, the presence of Aβ is insufficient for AD pathogenesis. Medical trials for drugs like BACE-1 inhibitors and solanezumab that target specific steps in the cascade have failed, producing either no effect or sometimes even worse cognitive function (Wessels et al., 2020; Honig et al., 2018). Additionally, a key study supporting the hypothesis that claims a form of Aβ as sufficient for inducing memory impairment was called into question in early 2022 over concerns about falsified data (Lesné et al., 2006; Piller, 2022). As a result of all of these factors, the cascade hypothesis has fallen out of favor in recent years. Although Aβ must be important, the prevailing view no longer considers it the sole root cause of AD. The search for a cause thus remains unresolved and holds invaluable insights into the disease.

*The Role of the Blood-Brain Barrier*

The answer may lie in the cardiovascular system, or rather, the brain's interface with the cardiovascular system: the blood-brain barrier (BBB). The BBB separates the blood circulating in the body from the central nervous system (CNS). It is semipermeable, meaning it bars harmful substances from entering the brain while allowing necessary substances in. In order to cross the BBB, molecules must be lipophilic and small, with molecular weights of 400 Da or lower (Teleanu et al., 2022). This quality of the BBB also makes it notoriously difficult for drugs targeting the brain, since they must make it past this barrier, placing restrictions on material and size. Microvessels and capillaries that supply blood to the brain are lined by endothelial cells that regulate permeability through intracellular junctions and passive and active transport (Zenaro et al., 2017). These endothelial cells make up the bulk of the BBB. Pericytes and astrocytes cover larger sections of the

BBB and establish additional intracellular junctions (Kubotera et al., 2019). The basement membrane surrounds endothelial cells and pericytes and further selectively regulates the passage of specific molecules (Muldoon et al., 1999). Neurons, microglia, and vascular smooth muscle also regulate the BBB, forming a larger, more comprehensive neurovascular unit (NVU) (**Fig. 1**), which consists of the BBB and everything that regulates it and the homeostasis of the CNS.

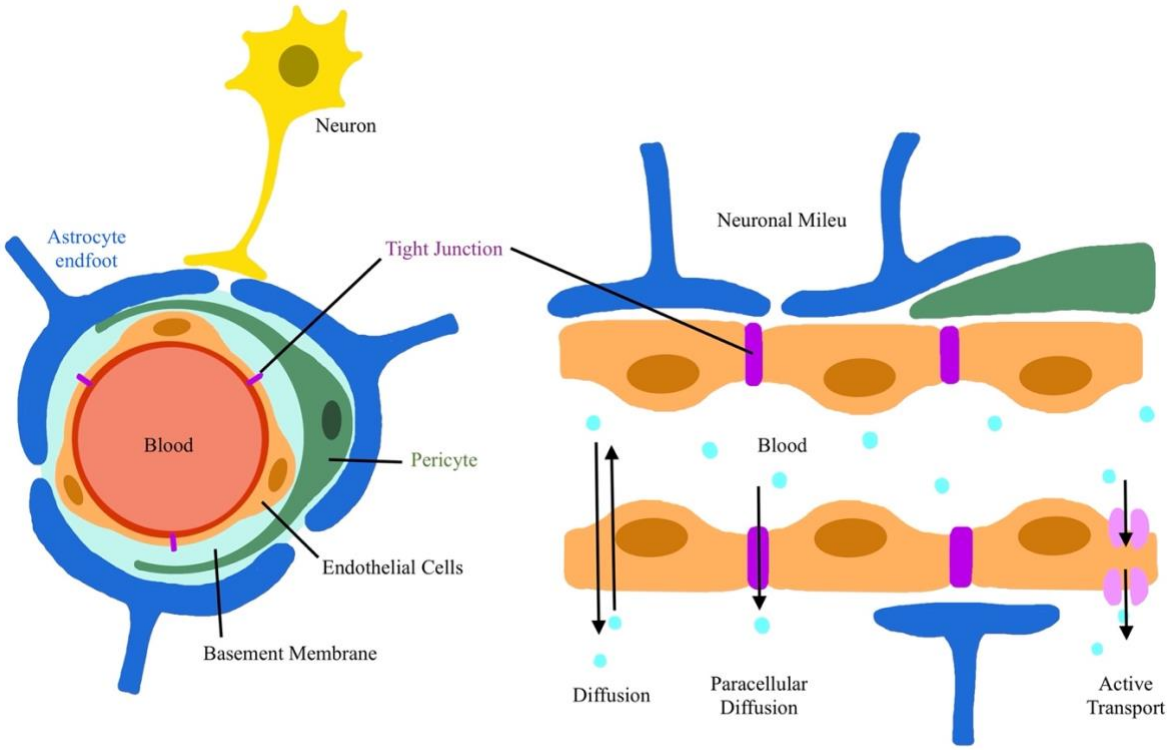


**Figure 1. A simplified model of the neurovascular unit (NVU).** The NVU is made up of the Blood-Brain Barrier (BBB) and associated elements that regulate it, such as the pericytes, astrocyte endfeet, and neurons. Substances traveling in the blood have more than one way of passing through the BBB to enter the environment of the CNS, called the "neuronal milieu." Passive diffusion is possible for extremely small molecules, and other some can even pass through the tight junctions in between endothelial cells through paracellular diffusion. Diverse active transport methods, from receptor-mediated endocytosis to facilitated diffusion, allow larger molecules to cross the BBB. Microglia, not shown here, are vital to maintaining the neural immune system and are also often included in the NVU. Vascular smooth muscle, also not shown here, regulates blood flow, and thus the flow of molecules, through contraction. Figure drawn using Procreate.

A dysfunctional BBB may interfere with proper clearance of Aβ from the CNS or may allow greater amounts of neurotoxic chemicals into the brain from peripheral circulation (Cai et al., 2018; Deane & Zlokovic, 2007). Receptor for advanced glycation end products (RAGE) proteins mediate transport of Aβ into the brain, while low-density lipoprotein receptor-related protein-1 (LRP1), a key receptor of ApoE, are primarily responsible for transport of Aβ from the brain to peripheral circulation (Donahue et al., 2006). AD is associated with aberrations in the behavior and distribution of RAGE and LRP1 in both the hippocampus and microvasculature (Donahue et al., 2006). A leaky BBB may also fail to prevent antibodies from entering the brain, resulting in increased immune response. This could explain the markers of neuroinflammation and glymphatic dysfunction often seen in AD brains (Scheltens et al., 2021). These toxic factors and responses can damage the BBB even further, accelerating the progression of the disease and magnifying its symptoms. BBB breakdown and neuroinflammation have been identified as key changes in early stages of AD and may interfere with proper synapse and neuron function, impair clearance of and promote aggregation of proteins like Aβ and tau, and promote microbleeds which contribute to oxidative stress (Sweeney et al., 2018; Erickson & Banks, 2013). Now, how the BBB begins to break down is yet another question. The Two-Hit Hypothesis posits that cardiovascular damage or dysfunction (the first hit) causes BBB breakdown which causes neuronal decay and neurotoxin accumulation. Henstridge et al. present a slightly different interpretation, suggesting that the buildup of Aβ and tau proteins early on in AD disrupts the BBB, which begins a vicious cycle of neurodegeneration and neurotoxic protein aggregation (Henstridge et al., 2019). Whatever the inciting incident may be, the BBB clearly plays a critical role in the pathogenesis, progression, and treatment of Alzheimer's and can provide additional insights independent of Aβ and tau. Furthermore, since these changes occur during early stages of AD, neurovascular imaging and other methods of assessing BBB integrity may improve diagnostic criteria.

*ApoE4 and the Blood-Brain Barrier*

ApoE4 is intimately linked with the decline of the BBB in AD. ApoE4 and ApoE4-related factors in the blood drive immune response-induced BBB breakdown, and the production of ApoE4 by astrocytes leads to dysfunction of the BBB (Riphagen et al., 2020; Jackson et al., 2022). Most important of all, ApoE4 causes BBB breakdown and can initiate cognitive dysfunction even without the presence of Aβ or tau protein (Montagne et al., 2020). ApoE4 destroys the BBB through multiple paths. It promotes the aggregation of fibrinogen in Aβ-rich areas, leading to blood clots (Hultman et al., 2013). It fails to suppress the proinflammatory cyclophilin A (CypA) metalloproteinase-9 (MMP-9) pathway in pericytes, which results in their degradation (Bell et al., 2012; Halliday et al., 2016). The CypA-MMP-9 pathway destroys the BBB and is moderated by the key ApoE receptor LRP1. While ApoE2 and ApoE3 interact with LRP1, ApoE4 has impaired interactions and is not able to properly regulate this pericyte-destroying pathway. ApoE4 also alters endothelial cell transport and destroys the basement membrane (Fullerton et al., 2001; Salloway et al., 2002). ApoE4 also results in the aberrant transport of Aβ, which could initiate or exacerbate AD pathology (Hultman et al., 2013).

*Implications for Treatment*

BBB breakdown has complicated implications for treatment and drug delivery. At first glance, an impaired BBB implies a leaky BBB, which can be the case since undesired factors can now cross over into the CNS. This would prove extremely beneficial for drug delivery and would remove some of the limitations that currently exist. However, the overarching cardiovascular dysfunction that caused the BBB breakdown can alter the structure and behavior of the neurovasculature. As the endothelial cells maintaining the BBB degenerate, water, ions, protein aggregates, and blood-derived substances can lodge themselves in the enlarged perivascular space of the deteriorating BBB, interfering with substance diffusion and transport (Sweeney et al., 2018). Additionally, immune

responses, altered transport mechanisms, and the likelihood of diffusing particles to get trapped in perivascular space all have the potential to further hinder attempts for drug delivery. Sweeney et al. suggest that to promote drug delivery, the damaged vasculature must first be stabilized and returned to their healthy diffusion-promoting state (Sweeney et al., 2018). This view contrasts with the simplified "leaky" BBB model, but acknowledging this nuance is critical to a better understanding of the BBB. Ultimately, BBB breakdown interferes with the carefully maintained homeostasis of the CNS, but further research must be done to untangle this web of processes.

*Measuring Blood-Brain Barrier Integrity*

To explore the extent of the deterioration of the BBB, we must develop a reliable assay to measure BBB permeability. The gold standard for studying BBB integrity involves Evans Blue dye (EB), a bright blue powder dye that fluoresces red at around 680 nm (Goldim et al., 2019; Hawkins & Egleton, 2005; Honeycutt & O'Brien, 2020). EB has a high affinity for albumin, so when introduced to the blood, nearly all of the EB molecules will bind with albumin protein. As a macromolecule, albumin cannot cross the BBB under normal circumstances, but a dysfunctional, leaky BBB will allow albumin and the EB bound to it through it. As a result, a greater degree of BBB breakdown and permeability will result in greater exposure to EB after perfusion. Perfusion is necessary to distribute the dye throughout the animal's body. A creature with a more dysfunctional, permeable BBB will have a bluer brain than normal. Most studies using EB homogenize the brains or extract EB protein using assays like TCA protein precipitation (Wang et al., 2018; Wang & Lai, 2014). However, to study where staining occurs and what regions, if any, were stained more than others, the brains must be sliced rather than homogenized, and slices must be imaged for EB fluorescence. A small handful of studies take this approach. Most of these studies aim not to visualize staining but to confirm EB as an effective assay for BBB permeability, but some find that EB leaks more in certain regions. The cerebellum, hippocampus, frontal cortex, thalamus, and

hypothalamus are identified as regions of high leakage (Sharma & Ali, 2008). While low molecular weight molecules evenly diffuse throughout the brain, high molecular weight molecules like albumin-bound EB enter most easily at the prefrontal cortex and cerebellum and least easily at the striatum, suggesting that the BBB exhibits alternate permeability patterns for molecules based on molecular weight (Yen et al., 2013). Most studies induce BBB breakdown or intracerebral hemorrhage through methods such as collagenase injection, focused ultrasound, or heparin (Manaenko et al., 2011; Yuanyuan et al., 2014; Ray & Keyrouz, 2014). Few studies have applied this method to study AD. Using EB-stained brain slices, Dickstein et al. found that immunization against Aβ restores BBB integrity, and Wang et al. demonstrated that APP-induced AD initiates cellular changes in the hippocampal NVU, leading to increased BBB permeability (Dickstein et al., 2006; Wang et al., 2011). This project will apply these methods to visualize how BBB permeability in regions across the brain are affected by ApoE4-induced AD.

*Thesis Objectives*

This thesis aims to characterize the breakdown of the BBB as associated with Alzheimer's disease. We will compare the degree of BBB permeability between an experimental group of AD model mice (ApoE4 group) and two control groups, one with a wild-type (WT) genotype and another with a neutral ApoE3 genotype, using an optimized Evans Blue dye protocol. Furthermore, the project will image and analyze slices of mouse brains to determine whether a pattern of staining exists and, if so, what regions of the brain are most affected by BBB breakdown. Higher degrees of staining indicate greater levels of BBB permeability and thus BBB breakdown. Regions with greater permeability are thus exposed to more harmful substances from the periphery or are less able to clear neurotoxic material. In short, the greater the amount of staining, the greater the impact AD is likely to have. This thesis will (1) characterize the pattern of staining within ApoE4 and control

brains and (2) test the following hypothesis: ApoE4 model mice exhibit statistically significantly greater BBB leakage than control mice ($P < .05$).

*Key Findings*

We found that if BBB permeability was disrupted, staining would be concentrated in the cortex, especially in the outer layers. Cortical areas with consistently high degrees of EB staining and thus BBB dysfunction were the primary somatosensory cortex, motor cortices, and piriform cortex. Hippocampal areas were also consistently stained, particularly in the dentate gyrus and CA1 stratum oriens. Small but dense regions of BBB disruption were located in areas between the hippocampus and thalamus. The substantia nigra pars reticulata exhibited significant BBB leakage only in ApoE4 brains. Due to the scarcity of literature studying its relationship to AD, it was identified as a region of interest for future study. Based on statistical analysis, we concluded that ApoE4 mice brains contain significantly more BBB disruption than WT and ApoE3 controls.

## Methods

*Genotypes and Mouse Selection*

Mice with the *ApoE4* transgene were selected as an experimental group modeling AD. AD-neutral *ApoE3* transgenic mice and wild-type (WT) genotype mice were selected as controls. WT mice were selected as a secondary control at the advice of Sinda Fekir to account for any possible variation in the brain caused by ApoE3. Although ApoE3 has been extensively documented as a AD-neutral variant of the *APOE* gene, we wanted to ensure that any difference observed in ApoE4 mice was significant and unique to the ApoE4 group. ApoE4 and ApoE3 mice were sourced from Taconic Biosciences (Rensselaer, NY), and the WT mice were obtained from the Jackson Laboratory (Bar Harbor, ME). All three groups consisted of 6 total mice, 3 male and 3 female, and were age-matched at 90 weeks old. The three groups will be age-matched to account for any natural

degradation of the BBB due to age, and old mice at 90 weeks of age were chosen to determine if AD-linked BBB breakdown is more severe or exhibits alternate patterns compared to BBB breakdown caused by aging. This project initially aimed to compare young and old groups as well, but due to time constraints, only the old group was studied. Grouping by sex was necessary to account for any risk factors associated with sex as observed in AD in humans, where women are at higher risk for AD than men. In total, 18 mice were involved in this experiment. All mouse lines were maintained in the Brown University Animal Care Facility, and all procedures were approved by the Brown University Institutional Animal Care and Use Committee.

*Evans Blue Injection*

EB was injected intravenously through the tail vein, which is the standard for Evans Blue BBB permeability assays. Evans Blue dye was prepared in a 0.3mL insulin syringe at a dosage of 200mg/kg of mouse weight, diluted in 0.1mL of sterile saline. The tail vein injections themselves were done by Sinda Fekir. Awake mice were constrained in a standard tail vein mouse tube. Their tails were taped into place over a custom-made tail holder that emits green light to illuminate the tail veins. Once secure, tails were swabbed with alcohol wipes to decrease the risk of infection and increase visualization of veins, and EB was then injected.

*Perfusion*

Perfusions were conducted an hour after injection to allow the dye to bind to albumin and circulate a bit throughout the mouse. Mice were anesthetized with 3% Isoflurane and 2% oxygen via a high-flow vaporizer anesthesia system for 5 minutes and then transferred to a perfusion tray, where a mask connected to the Isoflurane vaporizer was placed around the muzzle. The pump was then changed to pump 2.5% Isoflurane and 1% oxygen for the duration of the perfusion. Toe pinches were performed to confirm anesthetic efficacy. The mouse was secured by its forelegs on

the tray with two 20-gauge needles. Incisions were made to expose the peritoneum, after which the pericardium was excised to gain access to the heart. A 27-gauge ¾-inch (0.4x19 mm) butterfly scalp vein needle was inserted into the lower left ventricle. The mouse was then perfused via syringe pumps with 20mL phosphate-buffered saline (PBS) at a flow rate of 6mL/min. Immediately after beginning the perfusion, the right atrium was cut. Perfusion with PBS was followed by 10mL of a 4% paraformaldehyde (PFA) solution at the same rate. The animals were then decapitated, and the brains were immediately extracted and placed into a 50mL centrifuge tube containing 20mL PFA solution and kept refrigerated at around 4°C. Within 24 hours, the brains were then transferred to a centrifuge tube containing 20mL 30% sucrose solution and kept refrigerated until slicing. Centrifuge tubes were wrapped in aluminum foil to minimize the interactions of light with EB's fluorescent properties.

*Brain Slicing and Cryotomy*

Brains were removed from the 30% sucrose and briefly and gently dried using laboratory task wipes before being wrapped in aluminum foil and stored in a -62°C freezer. Pictures were taken of the brains before and after storage in the freezer for qualitative analysis. After 30 minutes or more, the brain was removed for slicing. Samples were mounted on chucks with OCT compound and were sliced into 20μm-thin coronal slices using a Leica CM3050 S cryostat machine. Slices were transferred from the machine into a 24-well plate filled with PBS using a paintbrush. To prevent cross-contamination of dye, separate brushes were used for each group of brains. Plates were then wrapped in aluminum foil and stored in a refrigerator at around 4°C.

*Slide Mounting*

Slices were placed in a petri dish filled with PBS and mounted on 75x25mm single-frosted microscope slides using a paintbrush. Separate petri dishes and brushes were used for each group to

prevent cross-contamination of dye. Two slides were made for each brain, one for slices including the striatum, primary somatosensory cortex (S1), and motor cortices, and one for slices including the entorhinal cortex and hippocampal region. The former group was referred to as the S Regions and the latter group the H Regions. The Allen Mouse Brain Atlas was referenced to determine the regions in each coronal slice. Each slide contained 6 slices. Slides were left to dry under aluminum foil for at least 30 minutes and were covered using #1.5 24x55mm coverslips and 35mL of Fluoromount without DAPI. After covering, slides were left under foil to dry for a day before being placed in a slide box.

*Imaging*

Slide boxes were delivered to the Leduc Bioimaging Facility (Providence, RI) for fluorescence imaging. 10x and 20x objectives were used, and imaging parameters were kept constant for all samples. Images were received in both VSI and JPEG file formats.

*Data Analysis*

Images of slices were analyzed using ImageJ. To correct for bias, slices were placed in folders according to the brain they originated from, and all names were removed. These folders were then randomly ordered from 1 to 18 by a third party. Slices were outlined using a polygon selection tool. The area inside the selection was analyzed for mean gray value, minimum and maximum gray value, and standard deviation. ImageJ calculates gray values by averaging the values of red, green, and blue pixels. Non-dyed pixels remained black, so mean gray values were taken as a measure of dye intensity. Box plots and statistical analyses were generated using GraphPad Prism 9. A one-way Kruskal-Wallis test was conducted to determine if any statistically significant difference existed across groups, and significance of the difference between means of experimental groups was determined in post-tests via Dunn's test, which also corrected for multiple comparisons in the

Kruskal-Wallis test. Gaussian distribution could not be assumed for the data. A P value of $P<0.05$ was accepted as statistically significant. Significance is indicated on graphs in the following manner: **** indicates $P \leq 0.0001$, *** indicates $P \leq 0.001$, ** indicates $P \leq 0.01$, * indicates $P \leq 0.05$.

## Results

### *Visualizing Staining*

In total, 18 brains, 36 slides, 216 slices, and 432 images (10x and 20x objectives) were reviewed and analyzed. This project selected two regions of interest. The first set of slices contained the striatum and multiple cortical areas, such as the S1 cortex and primary and secondary motor areas. These were called the S Regions and were characterized by more medial fang-shaped or U-shaped lateral ventricles. The other set, called the H Regions, included the hippocampal formation and entorhinal cortex. Degree of staining varied widely but overall was not dependent on how rostral or caudal a region was located. Outer cortical regions of the brain were consistently highly stained, and in most mice, the internal structures were dimly stained or not stained at all (**Fig. 2-4, 6**). Some female samples showed high leakage levels, causing staining of even these internal areas.

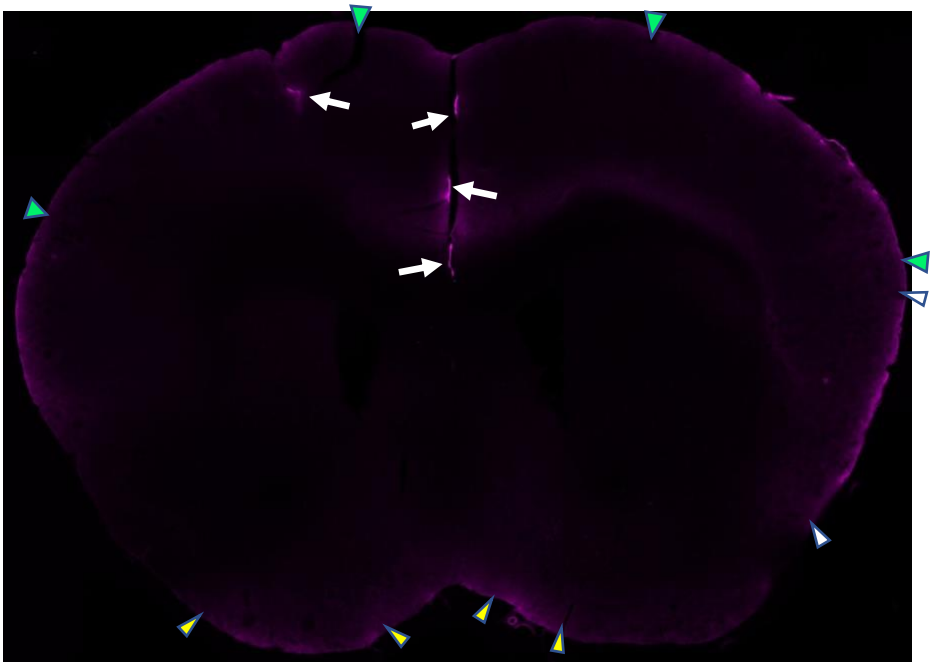

**Figure 2. Coronal rostral S region section from a male ApoE4 mouse.** Outer layers of the cortex are brightly stained, while the internal structures are inscrutably dark. Parts of the primary somatosensory cortex (S1), bounded by the green triangles, and gustatory and piriform cortices, bounded by the white triangles, here have high degrees of

staining. The olfactory tubercule, bounded by yellow triangles, is also stained. Note the small, dense region of staining within S1 and the stained areas in the sagittal fissure indicated by the white arrows.

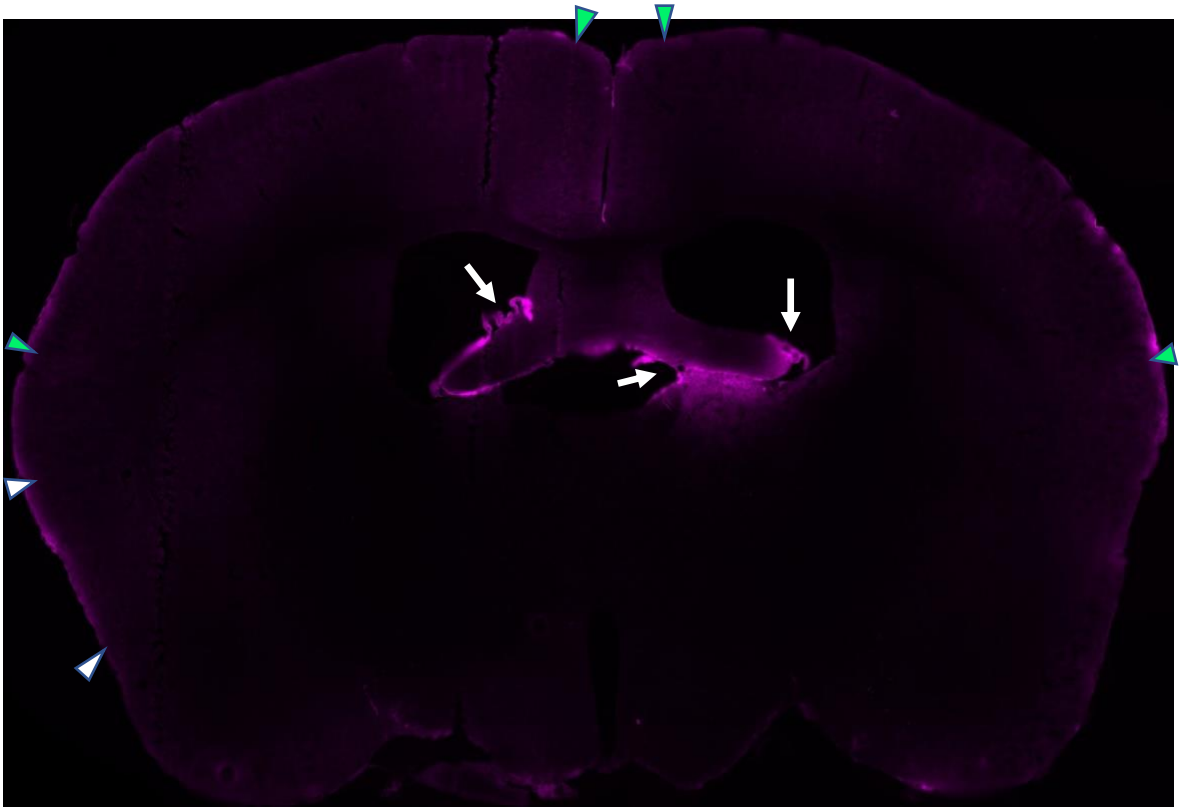

**Figure 3. Coronal caudal S region section from a male ApoE4 mouse.** S1, primary motor, and secondary motor areas (bounded by green triangles) and piriform cortex (white triangles) are particularly stained. Additionally, the lining of the ventricles around the fornix is highly stained, indicated by the white arrows.

Ventricular lining was most often stained near the fornix, fimbria, and hippocampus (**Fig. 3-5**). The hippocampal formation was also consistently stained, especially within the hippocampus itself and the region between the hippocampus and thalamus. Notable, frequently highly stained regions were the dentate gyrus and the stratum oriens of the hippocampal CA1 area (**Fig. 5-7**). The cortex was stained throughout, including areas like visual and auditory cortices and entorhinal cortex, but no one cortical area was consistently stained more than other areas. As the slices became more caudal, the substantia nigra pars reticulata (SNr) also revealed itself as a highly stained region of interest, but only in slices from ApoE4 animals (**Fig. 6, 7**).

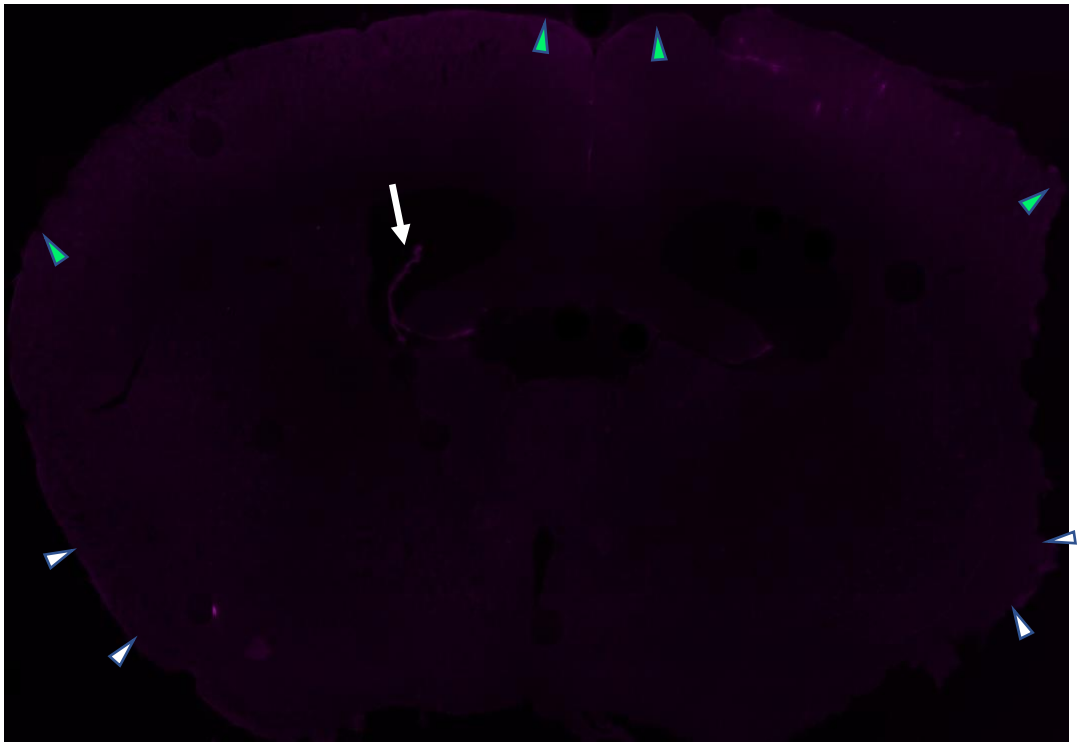

**Figure 4. Coronal caudal S region section from a female WT mouse.** Though staining is dim overall, cortex is visibly more stained than the internal structures. S1 and motor cortices (bounded by green triangles) and piriform cortex (white triangles) are all included within the stained regions. Ventricular lining (white arrow) is also stained.

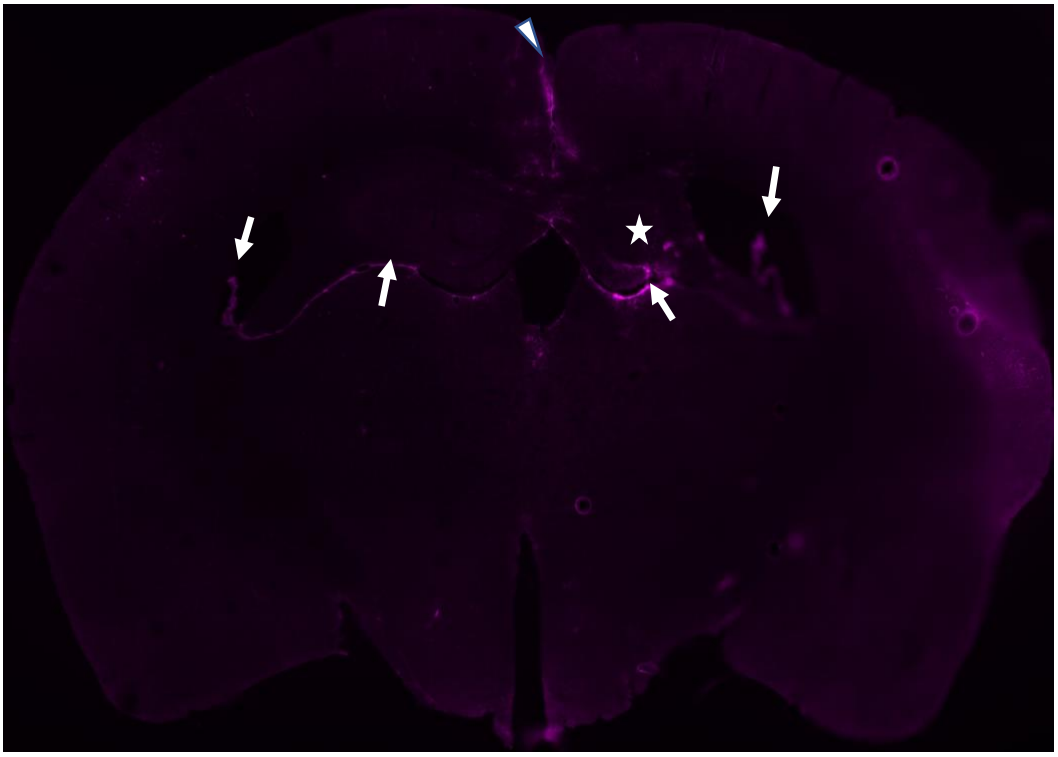

**Figure 5. Coronal H region section from a male ApoE4 mouse.** The greatest density of staining here occurs in the sagittal fissure (white triangle) and in the lining of the ventricles around the hippocampus and fimbria (white arrows). Some staining even seeps into the dentate gyrus at the border between hippocampus and thalamus (white star).

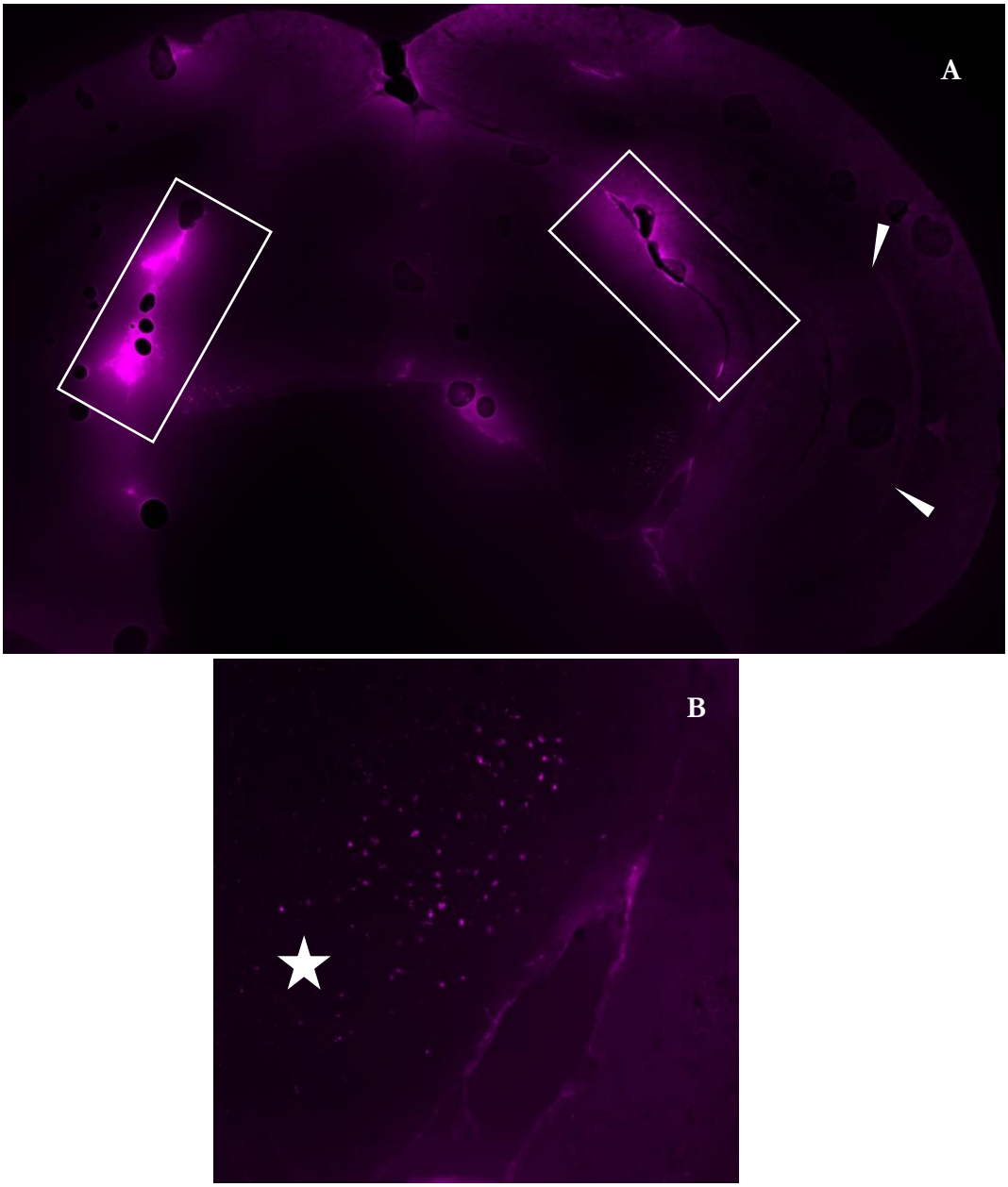


**Figure 6. Coronal caudal H region section from a female ApoE4 mouse.** This mouse had a hematoma which ablated the lower left area of this slice and could explain the degree of dye seen in the left hemisphere. **(A)** The greatest density of staining in both hemispheres occurs in the boxed regions, between the hippocampal formation and thalamus or midbrain. Cortex is also more brightly stained than to the internal structures of the midbrain. Hippocampal CA1 stratum oriens (white triangles) is also slightly more brightly stained than its neighbors, although the more medial regions of the hippocampus like the molecular layer of the dentate gyrus are the most brightly stained out of the whole hippocampal formation. **(B)** The substantia nigra pars reticulata (SNr) were also brightly stained (white star).

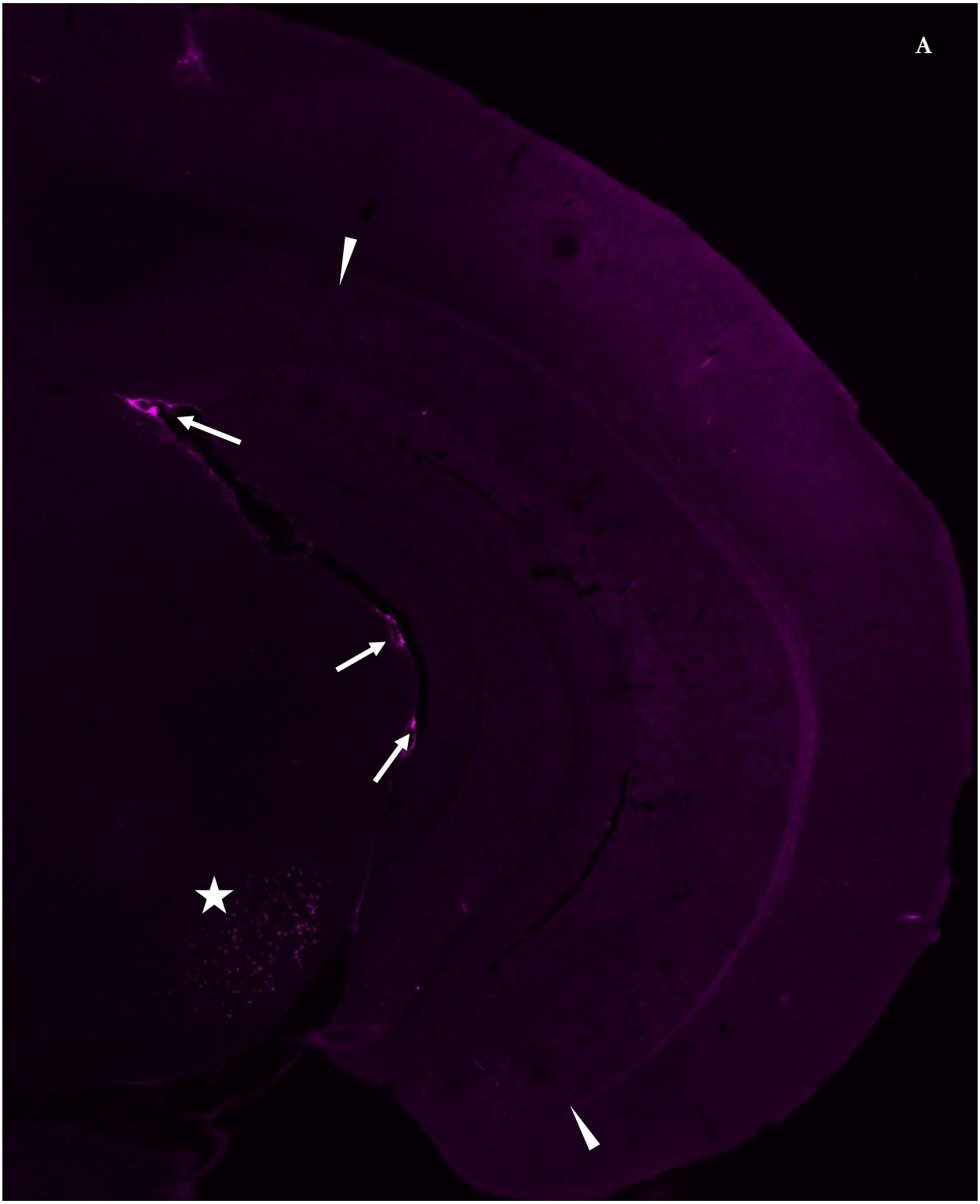
A

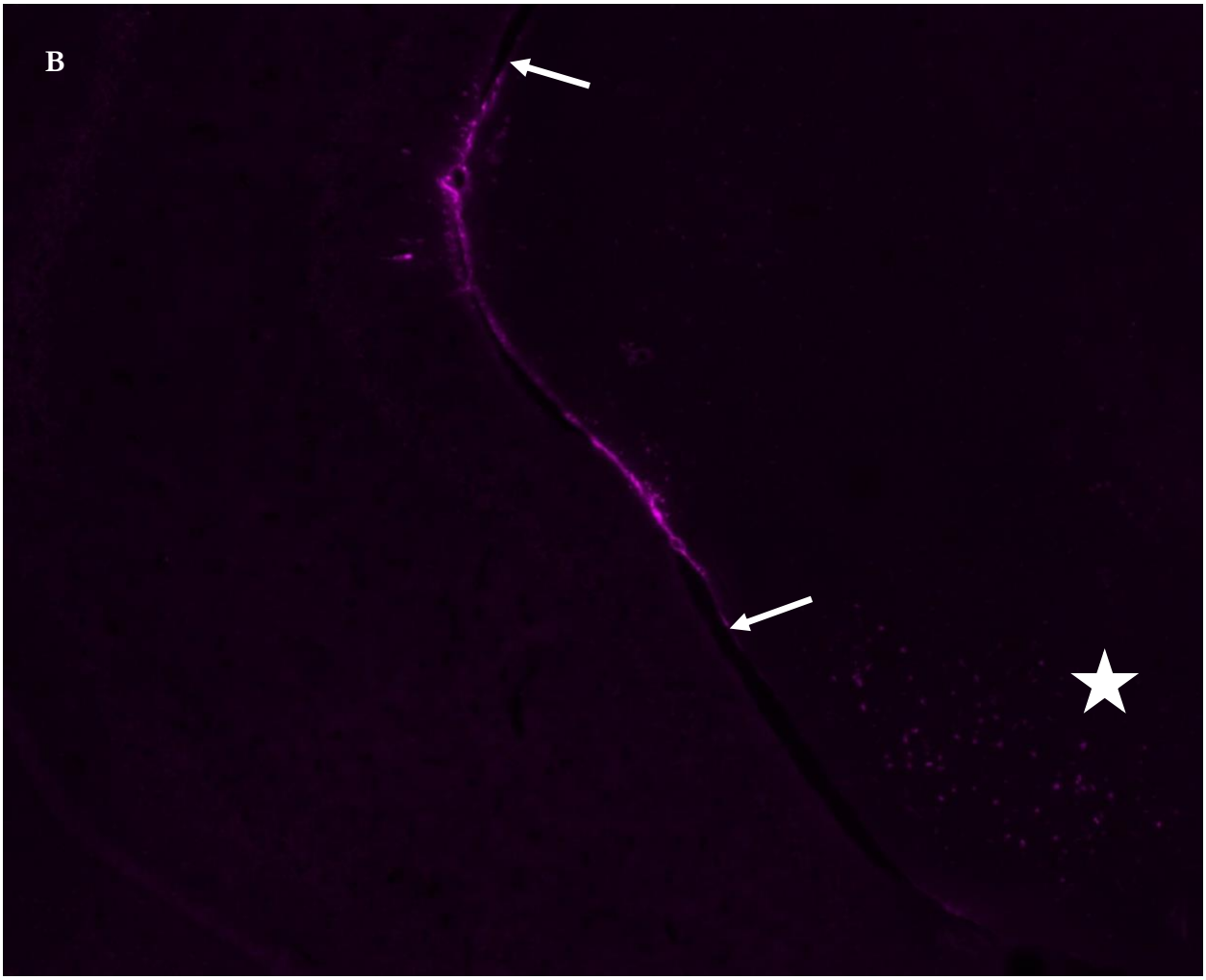


**Figure 7. Coronal H region sections from a male ApoE4 mouse.** The right hemisphere **(A)** is more brightly stained in this mouse and reveals the high degree of staining of the cortex and hippocampus. The midbrain is comparatively dim, except for pockets of dense staining between the hippocampus and thalamus and hippocampus and midbrain (white arrows). The hippocampal CA1 stratum oriens is brightly stained (bounded by white triangles). The left hemisphere **(B)** demonstrates extensive, bright staining in the narrow region between the hippocampus (left) and thalamus (right) (bounded by white arrows). Significant staining is also present in the SNr of both hemispheres (white stars).


**Figure 8. Visual comparison of representative brains.** Photos of brains were taken after freezing and before slicing. Although the phone camera quality and lighting washes out the blue coloration, some is still visible. In clockwise order starting from **(A):** WT female, ApoE3 female, ApoE4 female, ApoE4 male, ApoE3 male, WT male. Black arrows point to spots of blue staining on the outside of the brains. Brains of controls (WT and ApoE3) did not display blue coloration, even if some were significantly stained inside.

Visually, whole ApoE4 mice brains were more visibly blue and more frequently blue compared to ApoE3 and WT mice (**Fig. 8**), and slices of ApoE4 brains were more likely to contain both denser regions of staining and more staining overall, but there were notable exceptions. Two ApoE4 mice, one male and one female, displayed aberrantly lower levels of staining, and one female ApoE3 mouse and two WT mice, one male and one female, displayed higher levels of staining. The aberrant male WT mice displayed extremely dilated ventricles and had a significantly decayed cortex (**Fig. 9**). The increased or decreased staining of the other four mice may be a result of experimental

error or of other AD-inducing or -preventing factors. Outlier tests were conducted, explained in the next section on quantitative results, but due to the small sample size, no samples were removed.

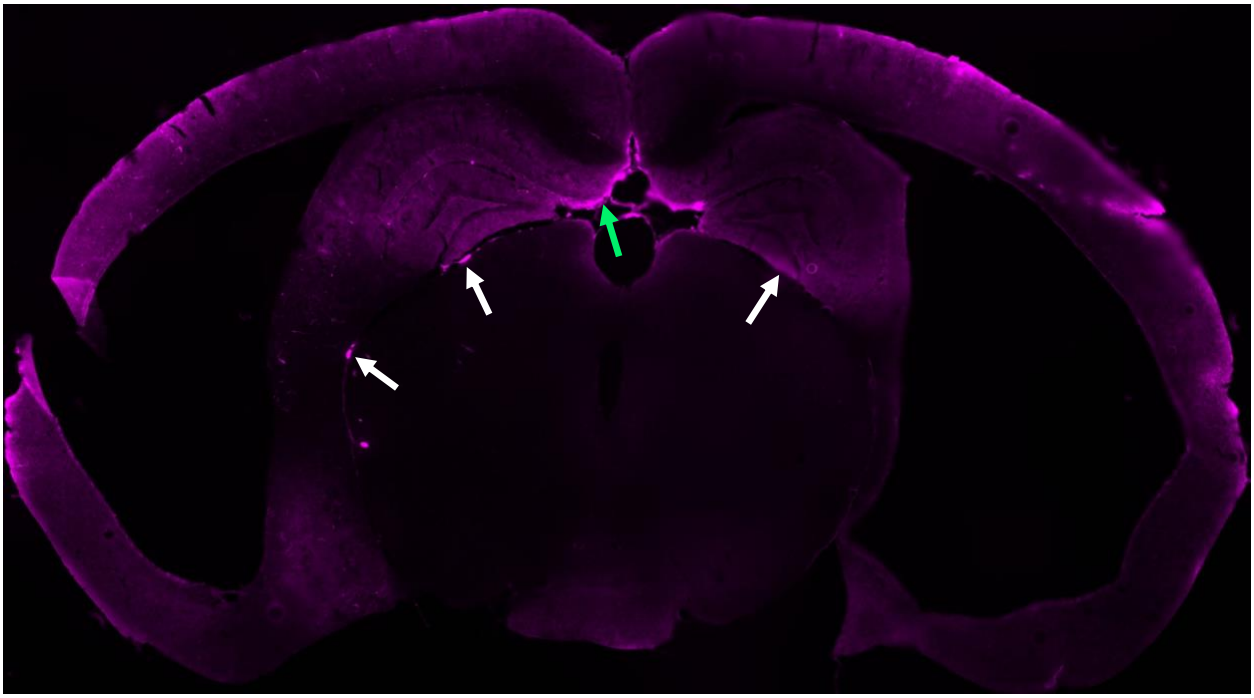

**Figure 9. Coronal rostral H region section from a male WT mouse.** Cortex and hippocampus are brightly stained. Outer cortex is densely stained, and staining encompasses nearly all of cortex, spanning S1, primary and secondary motor cortices, auditory cortices, entorhinal cortex, and piriform cortex. Lining of the third ventricle is also brightly stained (green arrow). The thalamus is dim, but pockets of dense staining exist between thalamus and hippocampus (white arrows). Large swathes of matter are missing, including sections of cortex and striatum, and the lateral ventricles are severely dilated.

*Comparing EB Intensity*

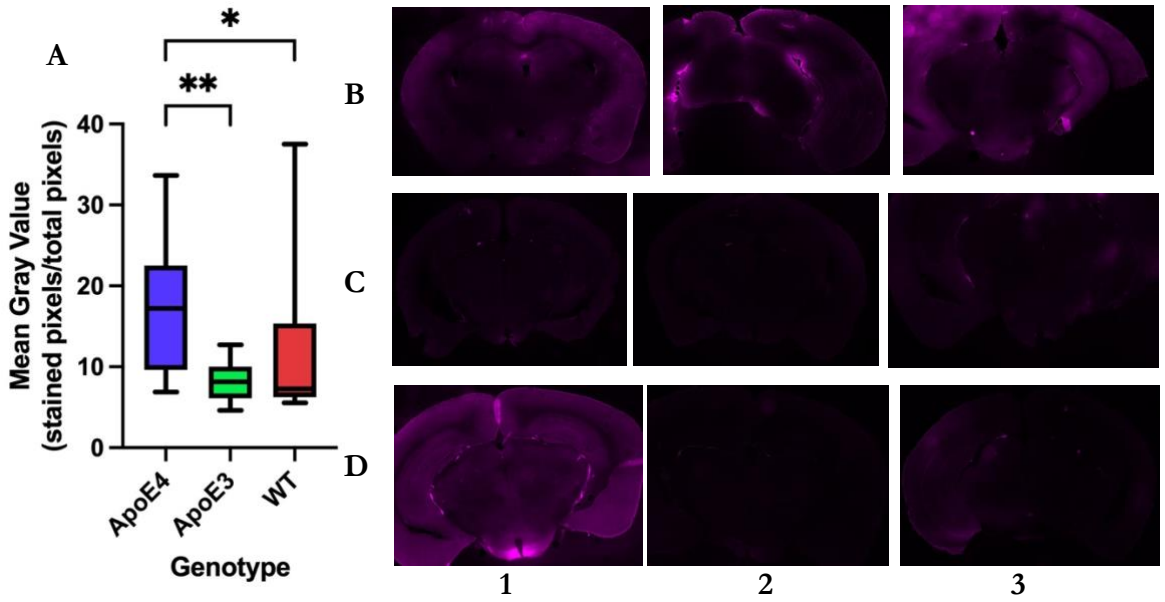


**Figure 10. EB intensity of female H regions. (A)** Slices were outlined and measured for mean gray value (MGV), representing intensity of EB staining, using ImageJ. Box-and-whisker plots were generated of the distribution of MGV across ApoE4 (blue; $n$ = 18 slices), ApoE3 (green; $n$ = 18 slices), and WT (red; $n$ = 18 slices) groups. Significant differences between groups was determined using one-way Kruskal-Wallis with Dunn's multiple comparisons post-testing. ApoE4 slices were significantly more stained than ApoE3 slices ($P$ = .001) and significantly more stained than WT slices ($P$ = .014). ApoE3 and WT groups were not significantly different ($P$ > .99). Representative images from each mouse brain are included in sections **(B-C)**. The **B** row indicates ApoE4 group brains, the **C** row indicates ApoE3 brains, and the **D** row indicates WT brains. Each column indicates a separate mouse within each group, numbered **1** to **3** from left to right (ie: the top left image is from the female ApoE4 mouse that was perfused first, notated as ApoE4 F1, while the top right image is ApoE4 F3).

First, the intensity of EB dye, represented by mean gray value (MGV), was obtained for each slice from all groups using ImageJ. MGVs were compared across ApoE4, ApoE3, and WT groups for each sex and each region of interest (H or S). We found significant differences in EB intensity between genotype groups within each sex-region group. For female H regions ($n$ = 54 slices), we found that the ApoE4 brains were stained more intensely than both ApoE3 and WT brains (**Fig. 10A**; $P$ = .001, $P$ = .014). ApoE4 brains had a median MGV of 17.2 (IQR 9.63-22.5), while ApoE3

and WT brains had median MGVs of 8.16 (6.12-10.0) and 7.27 (6.25-15.4), respectively. Due to the possible presence of outliers and inability to assume normal distribution, median and interquartile range (IQR) was evaluated rather than mean and standard deviation. Additionally, Kruskal-Wallis and Dunn's test compare medians rather than means. The IQRs of each group indicate that ApoE3 brains (IQR = 3.88) displayed less variability in mean gray value than ApoE4 (IQR = 12.9) and WT (IQR = 9.15) brains. Female ApoE4 H region slices were more visibly stained than all other female H region groups except for one WT brain (**Fig. 10B-D**). Cortex and hippocampus were highly stained (**Fig. 10B**, **D1**), and staining around the ventricles (**Fig. 10B1**) and on the border between hippocampus and thalamus (**Fig. 10B2-3**, **C3**, **D1**) was common. All ApoE3 and most WT H region slices were extremely dim, although light staining can be made out in the cortex and hippocampus (**Fig. 10C**, **D3**). Even when hippocampal staining is not visible or present, light cortical staining usually is (**Fig. 10C2**). Some of the brightest mean gray values (MGV = 37.5, 36.8) in any sample in this experiment were seen in the WT F1 brain. Even among this bright staining, the remarkably bright regions between the hippocampus and thalamus still stand out, as does this animal's hypothalamus (**Fig. 10D1**).

Female S region brains ($n$ = 54 slices) showed similar results, with ApoE4 brains having statistically significantly higher EB intensity than both ApoE3 and WT brains (**Fig. 11A**; $P$ = .032, $P$ = .006). The distribution of ApoE4 samples had a median MGV of 12.9 (IQR 8.57-24.8), which was higher than the median ApoE3 MGV of 7.48 (5.69-12.0) and median WT MGV of 5.98 (5.28-12.8). WT and ApoE3 brains displayed no significant difference (**Fig. 11A**; $P$ > .999). Unlike the H regions, ApoE3 (IQR =6.31) and WT (IQR = 7.52) brains were similarly variable, while ApoE4 brains continue to display high variability (IQR = 16.2). ApoE3 F2 may be an outlier, which would explain the high maximum observed in the data (MGV = 33.3) despite low overall MGVs for all other ApoE3 slices. However, due to the small sample size of animals, we hesitate to define it as

such and remove it from the data. It is worth noting that the S regions of the ApoE3 F2 brain are brightly stained while the H regions are barely visible (**Fig. 10C**, **11C**). Conversely, ApoE4 F3, which had bright H region slices, had very dim S region slices (**Fig. 10B**, **11B**). Overall, ApoE4 female S region slices were visibly brighter and more intensely stained than ApoE3 and WT S region slices (**Fig. 11B-D**). Continuing trends among these images are brightly stained cortices, particularly in the outermost layers (**Fig. 11B**, **C2**, **D1**). Although staining occurs throughout multiple cortical areas, slices from the ApoE4 group tended to show dense, bright regions of staining in the S1, motor, and piriform cortices (**Fig. 11B**). Ventricular lining, especially around the fornix, was also often brightly stained (**Fig. 11D1**).

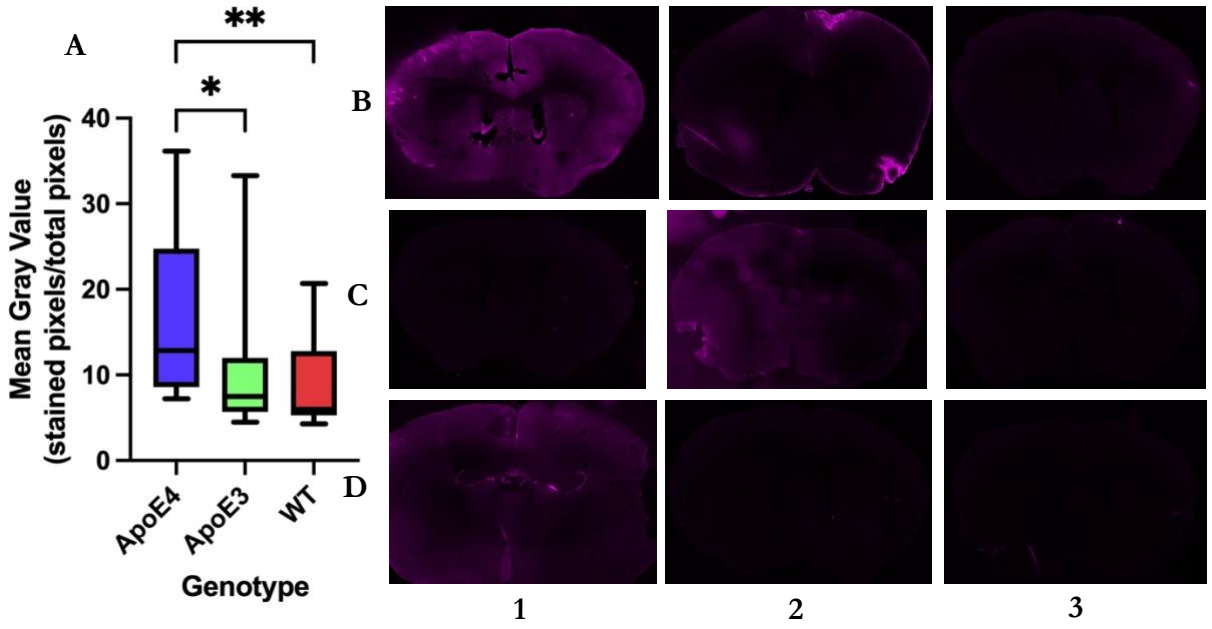


**Figure 11. EB intensity of female S regions. (A)** MGVs were compared across ApoE4 (blue; *n* = 18 slices), ApoE3 (green; *n* = 18 slices), and WT (red; *n* = 18 slices) groups. ApoE4 slices were significantly more stained than ApoE3 slices (*P* = .032) and significantly more stained than WT slices (*P* = .006). ApoE3 and WT groups were not significantly different (*P* > .99). Representative images from each mouse brain are included in sections **(B-C)**. The **B** row indicates ApoE4 group brains, the **C** row indicates ApoE3 brains, and the **D** row indicates WT brains. Each column indicates a separate mouse within each group numbered **1** to **3**.

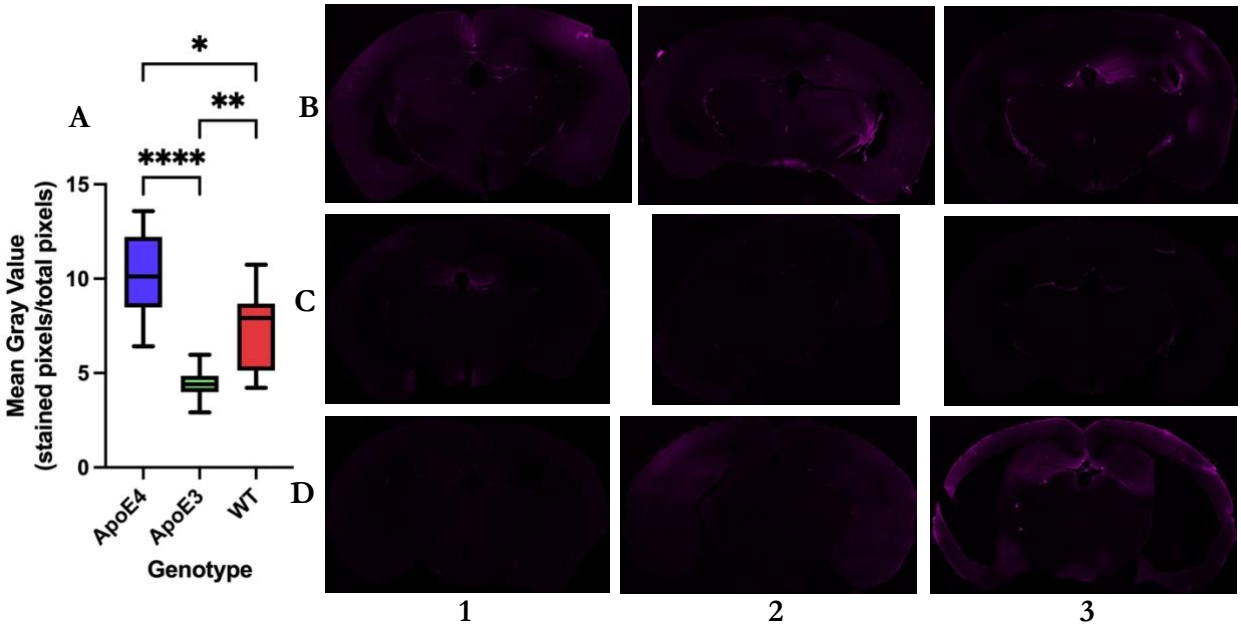


**Figure 12. EB intensity of male H regions. (A)** MGVs were compared across ApoE4 (blue; $n$ = 18 slices), ApoE3 (green; $n$ = 18 slices), and WT (red; $n$ = 18 slices) groups. ApoE4 slices were significantly more stained than ApoE3 slices ($P < .0001$) and moderately significantly more stained than WT slices ($P = .045$). ApoE3 and WT groups were also significantly different, with WT being more stained ($P = .002$). Representative images from each mouse brain are included in sections **(B-C)**. The **B** row indicates ApoE4 group brains, the **C** row indicates ApoE3 brains, and the **D** row indicates WT brains. Each column indicates a separate mouse within each group numbered **1** to **3**.

The Male H region had $n$ = 54 slices. ApoE4 brains displayed significantly more EB leakage than both ApoE3 and WT brains (**Fig. 12A**; $P < .0001$, $P = .045$). Median ApoE4 MGV was 10.1 (IQR 8.48-12.2), which was higher than the median WT MGV of 7.92 (5.14-8.68) and much higher than the median ApoE3 MGV of 4.41 (3.99-4.85). Unlike the female data, however, the WT brains were also more stained than the ApoE3 brains (**Fig. 12A**; $P = .0015$). Both ApoE4 (IQR = 3.74) and WT (IQR = 3.54) brains were more variable than the ApoE3 (IQR = 0.86) brains, although all groups were less variable than their female counterparts. Many of the male samples seemed dimmer than the female brains despite being imaged with the same parameters. Despite the dimness, the ApoE4 samples were consistently more stained (**Fig. 12B-D**) than the two controls. Outer cortex was almost always stained, especially dorsal areas (S1 and motor cortices) (**Fig. 12B1**, **B3**, **D2**-**3**).

The hippocampal formation was frequently stained as well, especially the dentate gyrus in rostral hippocampal sections (**Fig. 12B1**, **B3**, **D3**) and the thalamo-hippocampal boundary in middle and caudal sections (**Fig. 12B2**, **B3**, **D3**).

The male S regions, $n$ = 54 slices, displayed significant increases in EB staining for both ApoE4 and WT brains compared to ApoE3 brains (**Fig. 13A**; $P < 0.0001$, $P < 0.0001$). However, there was no significance between ApoE4 and WT groups (**Fig. 13A**; $P = 0.52$). Median MGV of ApoE4 brains was 7.47 (IQR 6.13-9.13), which was similar to the median WT MGV of 6.32 (5.13-7.58). Both were higher than the median ApoE3 MGV of 4.02 (3.70-4.29). The ApoE3 IQR, 0.59, remained consistent with the narrow IQRs observed for all other ApoE3 data, although the female S region data contained some uncharacteristically high datapoints contributing to its wide whiskers (**Fig. 11A**). ApoE4 (IQR = 3.00) and WT (IQR = 2.45) variabilities were similar, and both were more variable than ApoE3 data. Overall, the male IQRs were much lower than the female IQRs. Like with other samples, outer cortex was more stained, especially in the dorsal areas (S1 and motor cortices) (**Fig. 13B**, **13D2**) and ventrolateral areas (piriform cortex) (**Fig. 13B3**, **13D2-3**). The inner structures, including the striatum, were generally unstained or extremely dim. The ventricular lining near the fornix was also frequently stained (**Fig. 13B3**).

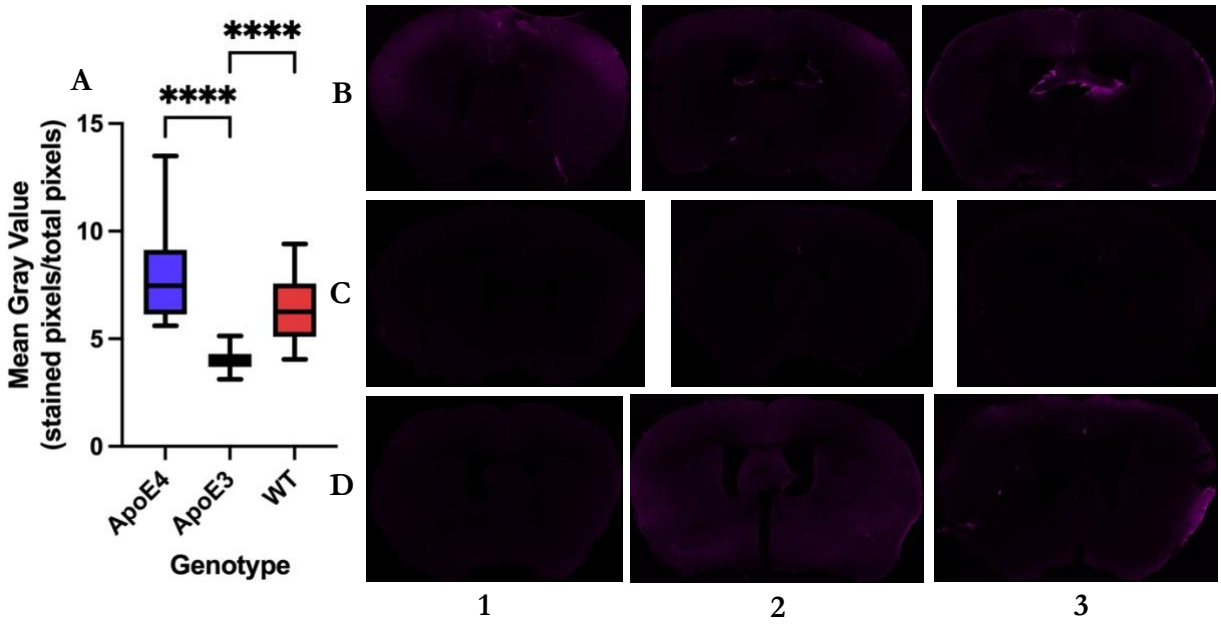


**Figure 13. EB intensity of male S regions. (A)** MGVs were compared across ApoE4 (blue; *n* = 18 slices), ApoE3 (green; *n* = 18 slices), and WT (red; *n* = 18 slices) groups. ApoE4 slices were significantly more stained than ApoE3 slices ($P < 0.0001$). WT brains were also significantly more stained than ApoE3 brains ($P < 0.0001$). However, ApoE4 and WT were not sigificantly different in intensity ($P = 0.52$), although they were near the .05 alpha value for significance. Representative images from each mouse brain are included in sections **(B-C)**. The **B** row indicates ApoE4 group brains, the **C** row indicates ApoE3 brains, and the **D** row indicates WT brains. Each column indicates a separate mouse within each group numbered **1** to **3**.

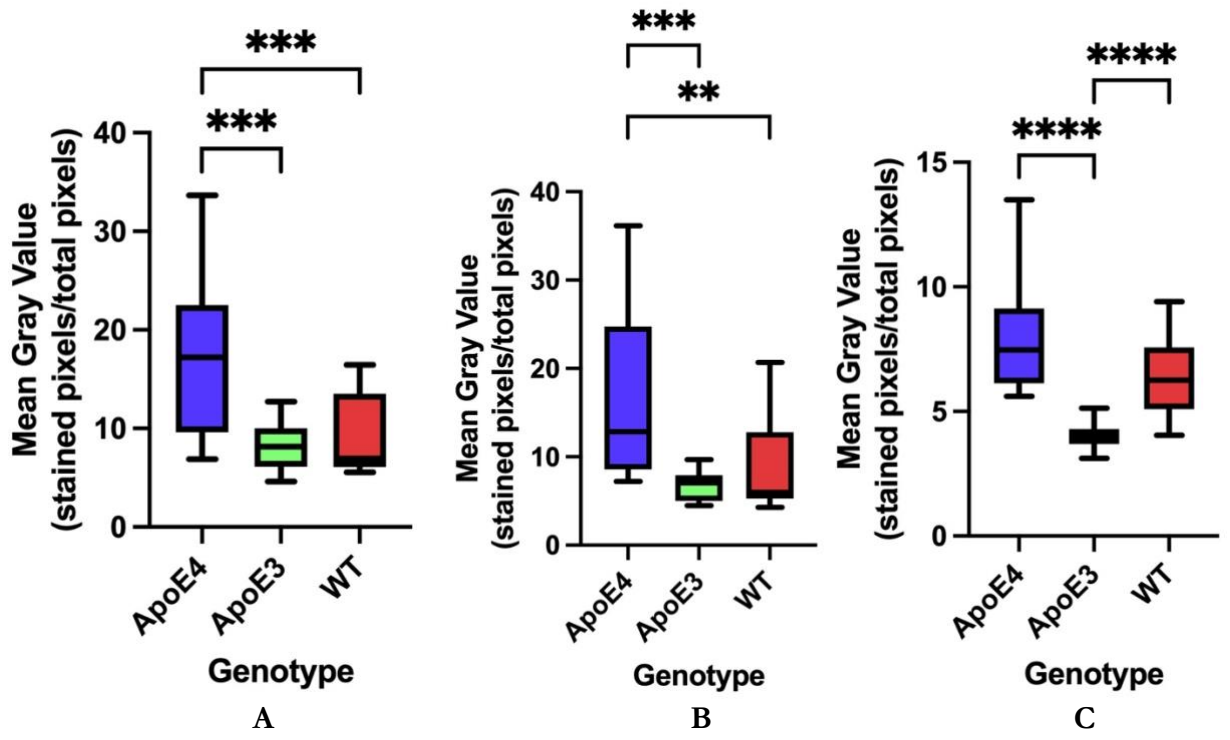


**Figure 14. EB intensity data accounting for outliers. (A)** Female H region data was found to have two outliers in the WT group. After removal, *P*-values decreased. The ApoE4 group was significantly more stained than the ApoE3 group ($P < .001$) and the WT group ($P < .001$). Any difference between WT and ApoE3 groups remained insignificant. **(B)** Four ApoE3 outliers were found in the female S region data. After removal, *P*-values decreased. The ApoE4 group was significantly more stained than the ApoE3 group ($P < .001$) and the WT group ($P = 0.002$). Any difference between WT and ApoE3 groups remained insignificant. **(C)** One WT outlier in the male S region data was found. When removed, the ApoE4-WT comparison had a *P* value = 0.11 and remained insignificant.

A robust regression and outlier removal (ROUT) test with an aggressiveness coefficient Q = 1% was used to determine the presence of outliers in the data. Following this, Kruskal-Wallis with Dunn's multiple comparisons testing was conducted on new data sets to determine the significance of differences between groups. Although we will not use this data because of the small sample size of the project, the outlier test was conducted to gain a deeper understanding of the datasets and pattern of staining intensity and to determine if some moderate significance was overlooked due to the p-value being marginally larger than the 0.05 alpha value. Two outliers were found in the female

H region data originating from the WT F1 mouse (MGV = 36.8, 37.5). If these outliers were removed, resulting in $n$ = 52 slices for the female H region and $n$ = 16 slices for the WT female H region data, no new significant differences would be found, but the significance of the difference between ApoE4 MGV data and ApoE3 and WT MGV data would increase (**Fig. 14A**). The *P*-value of the ApoE4-ApoE3 comparison decreased from $P = .001$ to $P < .001$, while the ApoE4-WT *P*-value decreased from $P = .014$ to $P < .001$. Four outliers were found in the female S region (MGV = (27.6, 33.3, 18.8, 20.2). These outliers all originated from the ApoE3 F2 mouse, which demonstrated visibly brighter staining than its other ApoE3 peers in qualitative image analysis. Removing these outliers, resulting in $n$ = 50 slices and $n$ = 14 slices for the ApoE3 subgroup, would also not introduce any new significant differences but would heighten the significance of the ApoE4-ApoE3 and ApoE4-WT differences (**Fig. 14B**). The *P*-value of the former would drop to $P < .001$ from $P = .032$, and the *P*-value of the latter would decrease to $P = .002$ from $P = .006$. No outliers were found in the male H region dataset, but one outlier from the WT M2 mouse (MGV = 12.8) was detected in the male S region data. Removing this datapoint (male S region group $n$ = 53 slices, WT subgroup $n$ = 17 slices) would not introduce any new significant differences (**Fig. 14C**). The ApoE4-WT comparison had a *P*-value of .11 and remained insignificant. The *P*-value of the ApoE4-ApoE3 and WT-ApoE3 comparisons remained $P < .0001$. Ultimately, no new significant differences were found even after removing outliers.

*Comparing EB Intensity Across S and H Regions*

Next, we wanted to characterize intensity variations across the brain, especially between S and H regions. We found no significant difference found between S and H regions in either females (**Fig. 15A**; $P = .90$) or males (**Fig. 15B**; $P = .53$). No significant difference in EB intensity between S and H regions existed within genotypes either. For female mice, ApoE4 H and S regions were statistically similar ($P > 0.99$), as they were for ApoE3 ($P > 0.99$) and WT ($P = 0.81$) genotypes (**Fig.**

**15A**). Male H and S region comparisons were also insignificant for ApoE4 ($P$ = .18), ApoE3 ($P$ = .90), and WT ($P$ = .51) genotypes (**Fig. 15B**).

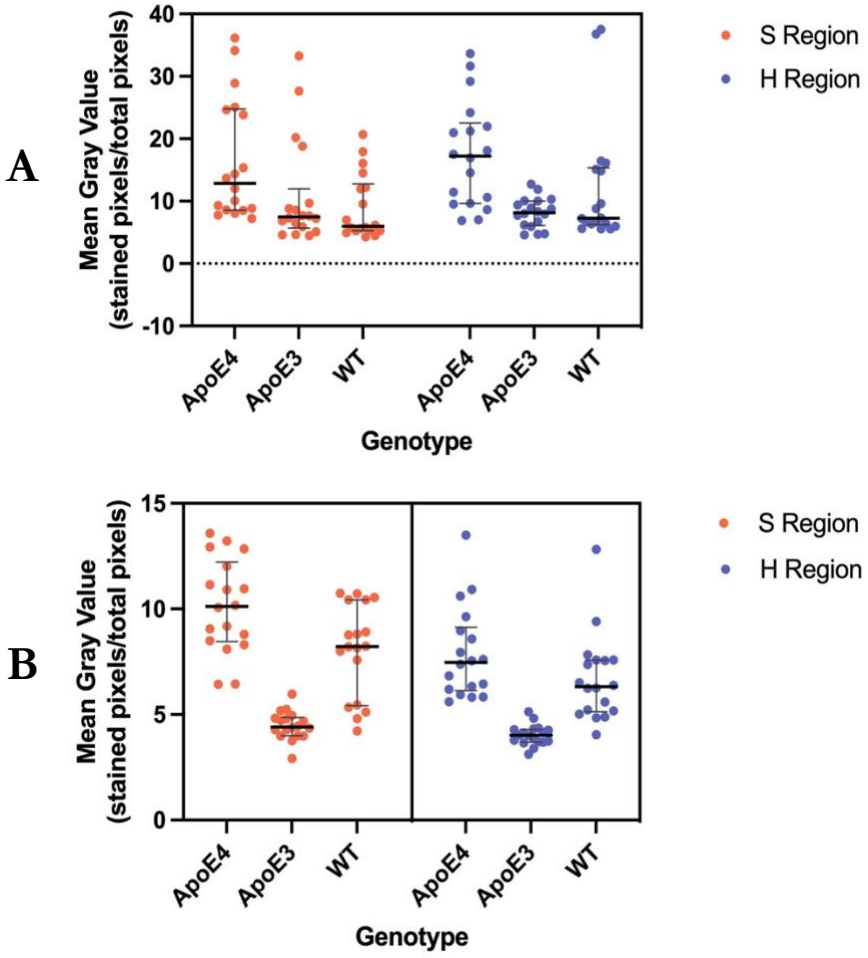


**Figure 15. Comparison of EB intensity in S and H regions.** Two datasets corresponding to sex were created from all MGV data. Data was grouped by region, either S (orange) or H (blue), and sub-grouped by genotype (ApoE4, ApoE3, WT). Scatterplots were generated. Black bars represent medians, and the gray whiskers represent IQRs. Mann-Whitney test was conducted to compare between all S region and H region data for each sex. Kruskal-Wallis with Dunn's multiple comparisons testing was all conducted on all MGV data to compare differences in regional staining within genotype groups. **(A)** Overall, females ($n$ = 108 slices) did not show any significant difference between regions ($P$ = .90). No significant difference was present within ApoE4 ($P$ > .99), ApoE3 ($P$ > .99), and WT groups ($P$ = .81). **(B)** Males ($n$ = 108 slices) also did not show any significant difference between S and H regions, both overall ($P$ = .53) and within genotype groups. No significant difference was present within ApoE4 ($P$ = .18), ApoE3 ($P$ = .90), and WT ($P$ = .51) groups.

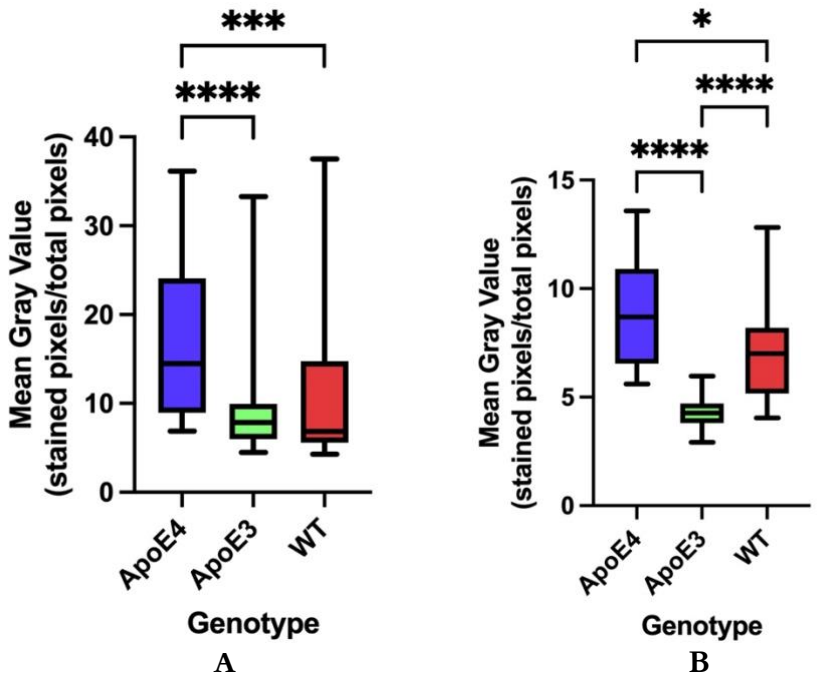


**Figure 16. EB intensity compared across ApoE4, ApoE3, and WT groups.** Box-and-whisker plots were generated of the distribution of all MGVs, both H and S regions, across ApoE4 (blue; *n* = 36 slices), ApoE3 (green; *n* = 36 slices), and WT (red; *n* = 36 slices) groups. Significant differences between groups was determined using one-way Kruskal-Wallis with Dunn's multiple comparisons post-testing. **(A)** Female ApoE4 brains were significantly more stained than ApoE3 ($P < .0001$) and WT ($P = .0001$) brains. ApoE3 and WT brains did not differ significantly ($P > .99$). **(B)** Male ApoE4 brains were significantly more stained than ApoE3 brains ($P < .0001$) and moderately significantly different from WT brains ($P = .04$). Male WT brains were significantly more stained than ApoE3 brains ($P < .0001$).

Since the difference between H and S regions was negligible, a comparison between ApoE4, ApoE3, and WT groups could be made of all the MGV data, regardless of region. In both the female (*n* = 108 slices) and male (*n* = 108 slices) cohorts, slices from ApoE4 animals were significantly brighter than ApoE3 slices (**Fig. 16**; $P < .0001$, $P < .0001$). Female ApoE4 slices had a median MGV of 14.5 (IQR 8.96-24.1), while female ApoE3 slices had a median MGV of 7.84 (6-9.94). Male ApoE4 slices had a median MGV of 8.69 (6.54-10.9), which was higher than the median male ApoE3 MGV of 4.23 (3.81-4.71). Both female and male ApoE4 brains were more stained than WT brains, but males showed only a moderately significant difference. (**Fig. 16**; $P = .0001$, $P = .04$).

Additionally, male WT slices were significantly brighter than male ApoE3 slices (**Fig. 16B**; $P < .0001$). The median female WT MGV was 6.85 (5.59-14.8), and the median for males was 7.01 (5.16-8.19).

Qualitative assessments of rostral versus caudal sections also varied widely, but there were no patterns or differences in overall degree of staining. Some regions were stained more in certain sections. For instance, the dentate gyrus contained more EB in more rostral sections of the hippocampus, possibly due to proximity to the third ventricle (**Fig. 5**, **9**). However, overall staining between rostral and caudal sections were relatively the same. An attempt to order sections and plot the relationship between EB intensity and rostral-caudal location was made, but slices were hard to empirically order due to the micrometer distance between slices making it difficult to decide which was more rostral or caudal in many cases.

*Comparing EB Intensity in Males vs Females*

Finally, we studied the difference between male and female brains. Male brain slices seemed much dimmer than female brain slices despite being prepared using the same procedures and imaged under the same parameters. To quantitatively assess this, one-way Kruskal-Wallis with Dunn's multiple comparisons testing was conducted on male and female datasets. Three graphs were generated, one for all data points, a second for H region slices, and a third for S region slices. No significance was found between WT male and female slices in any region (**Fig. 17**). However, ApoE3 data consistently showed differences between males and females, with females being more intensely stained ($P < .0001$). Slices from ApoE3 females were brighter in both H regions ($P < .001$) and S regions ($P < .0001$) (**Fig. 17**). Female ApoE4 brains were moderately significantly more stained than male brains in the S region ($P = .04$) but were not significantly different from male brains in the S region (**Fig. 17**). Overall, however, female ApoE4 brains were significantly more stained than male ApoE4 brains (**Fig. 17A**; $P = .01$). Female ApoE4 brains showed the highest

degree of staining, with a median of 14.5 (8.96-24.1), and male ApoE3 brains showed the least, with a median of 4.27 (3.81-4.71).

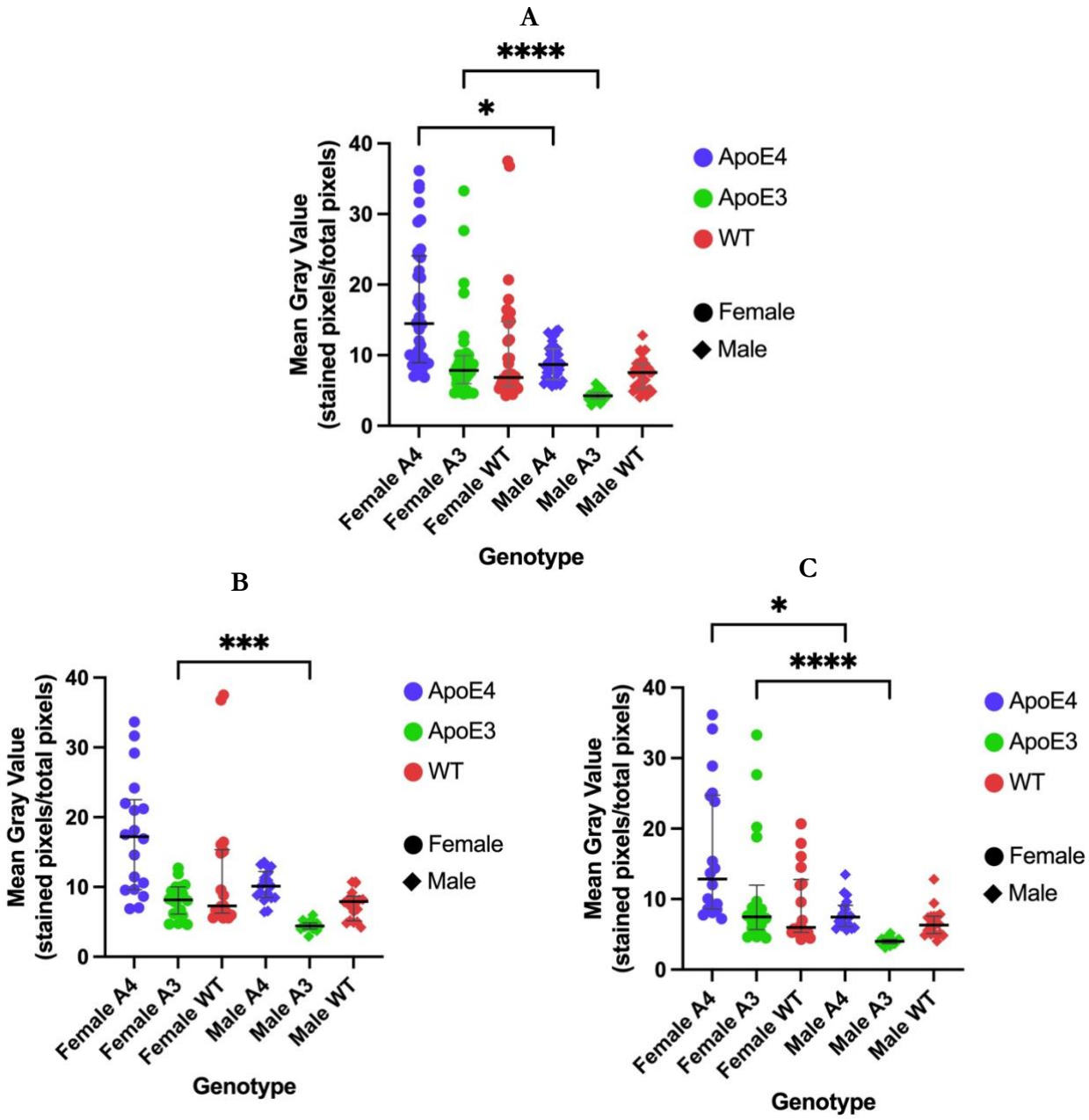


**Figure 17. Difference in EB intensity by sex.** Scatterplots were generated of all ApoE4 (blue), ApoE3 (green), and WT (red) slices from **(A)** both regions, **(B)** H regions only, and **(C)** S regions only. Black lines represent medians and gray whiskers represent IQRs. Males (diamonds) and females (circles) were compared within each genotype group. **(A)** Female slices were significantly brighter than male slices for ApoE4 ($P = .01$) and ApoE3 ($P < .0001$) genotypes. WT

slices did not vary significantly based on sex ($P = .37$). Similarly, **(B)** female ApoE3 slices taken from the H region were significantly brighter than male ApoE3 H-region slices ($P < .001$). WT H-region slices did not vary significantly based on sex ($P = .58$), and neither did H-region slices from ApoE4 ($P = .39$). **(C)** Female ApoE4 slices from the S region had moderately significantly higher MGVs than their male counterparts ($P = .04$). Female S-region ApoE3 slices had significantly higher MGVs compared to males ($P < .0001$). EB intensity for WT slices did not vary by sex ($P > .99$).

## Discussion

### *Characterizing the impact of AD on the brain*

The first purpose of our study was to visualize and characterize the degradation of the BBB across multiple regions of the brain. We found a consistent, high degree of staining in the outer layers of the cortex throughout visualized brain slices, which suggests a high degree of BBB permeability and AD pathology localized at these regions. Even when other structures remain unstained or dim, cortex remains relatively stained. This may indicate that cortex is more severely impacted by BBB permeability or that it is impacted before other structures. Recent research suggests that somatosensation may not be spared by AD as previously thought. Wiesman et al. found that AD significantly affects somatosensory function, although this dysfunction is frequently hidden by the cognitive decline symptoms in AD patients (Wiesman et al., 2021). AD also affects motor control through killing and changing the neurons and neural environment of motor areas, especially primary motor cortex (Suvá et al., 1999; Salazar et al., 2019). Dorsal areas corresponding to S1 and primary and secondary motor cortices were frequently stained, which may suggest that the BBB is particularly vulnerable in these areas. Additionally, ventrolateral areas of S region slices corresponding to the piriform cortex were also often stained. Early symptoms of AD include an impaired sense of smell, which has been attributed in part to the disruption of neural coding of odors in the piriform cortex (Murphy, 2019; Li et al., 2010; Saiz-Sanchez et al., 2011). Some slices

displayed staining of the olfactory tubercule (**Fig. 2**), which is also involved in olfaction. Olfactory regions seem to be frequent targets of BBB dysfunction and leakage.

Most internal structures remained quite dim, aside from a few exceptions. The lining of the lateral ventricles was unstained everywhere except near the fornix, the major output white-matter tract of the hippocampus. This further supports the vulnerability of the hippocampal formation to BBB leakage. The fornix is crucial to limbic and behavioral processes and has been identified as a promising target for deep brain stimulation (DBS) therapies to improve cognitive function (Ríos et al., 2022). Changes in and degeneration of the fornix may play vital roles in the conversion from mild cognitive impairment to clinical AD (Oishi & Lyketsos, 2014). Another rarely but highly stained internal structure was the substantia nigra pars reticulata (SNr), which was strangely only stained in ApoE4 animals. Not much discussion of a link between the SNr and AD exists, but the SNr is key to behavioral regulation, which may implicate it somewhat in the decline of cognition. Additionally, SNr neurons are primarily GABAergic, and GABA may be involved in AD and cognitive dysfunction. Low GABA levels have been detected in severe cases AD, and dysfunctional GABA may be associated with cognitive impairment (Xu et al., 2020; Solas et al., 2015; Murari et al., 2020). Further research must be conducted into the role of the SNr in AD, as this area has been identified in this analysis as one with a high degree of BBB dysfunction. As indicated by prior research, the striatum was rarely ever stained, reflecting the differential permeability of the BBB to high- and low-molecular weight substances (Yen et al., 2013).

The hippocampus was also consistently stained across all groups, but especially in ApoE4 groups. Two main areas of interest were identified. The first is the dentate gyrus, which has been extensively studied and long been identified as a key region in AD. The dentate gyrus is involved in associative memory and would be an important target for a memory-affecting disease like AD. Tau proteins have been shown to aggregate in dentate gyrus astrocytes and cause cognitive impairment

and widespread neuron death (Richetin et al., 2020). Additionally, dentate gyrus cell structure changes in association with the progression of AD (Valadez et al., 2022). The second key area is the CA1 stratum oriens. Seen in many ApoE4 slices as a thin, brightly stained line in between the dim CA1 pyramidal cell layer and the unstained alveus, the stratum oriens is one of the brightest stained structures within the hippocampus. The stratum oriens is also highly studied in AD research. It is a region of significant Aβ and tau aggregation, and tau pathology here is critical for the progression of dementia symptoms (Mizuta, 2023; Takamura et al., 2021; Thal et al., 2000). Finally, while not a region of the hippocampus itself, some of the most brightly stained areas in the H regions were regions between the hippocampus and the thalamus. Thalamic nuclei are each affected by AD in different ways, and the specific nuclei and pathways involved in these staining patterns are unclear (Pardilla-Delgado et al., 2021). Further investigation must be done to understand the significance of this staining. Ultimately, the fact that all of these areas associated with AD demonstrate high staining shows that BBB breakdown is reliably associated with the changes happening in AD.

*The BBB in ApoE4 mice is significantly more disrupted than in controls*

The second purpose of our study was to determine whether ApoE4 model mice exhibit statistically significantly greater BBB leakage than control mice. We found that ApoE4 brains were significantly brighter and contained more dye than ApoE3 and WT brains, indicating that the BBB exhibited increased permeability in the ApoE4 animals (**Fig. 16**). This was the case regardless of the sex of the animal and the region the slice had been taken from. Thus, ApoE4 does indeed induce BBB dysfunction as predicted by studies like Montagne et al., and ApoE4 increases the risk of undesired substances entering the CNS, resulting in the characteristic patterns of staining described in the previous section (Montagne et al., 2020). Our findings add further evidence to the importance of the BBB in AD etiology and pathology.

The anomalous decreased significance for male ApoE4-WT comparisons may have been in part due to data from the WT M3 mouse, which exhibited enlarged ventricles and decayed neural tissue, characteristic signs of neurodegeneration. Slices from this animal exhibited slightly higher MGVs compared to slices from the other two WT animals. The ROUT outlier test could not account for most of the outliers originating from this animal because we did not use a statistical method designed to handle clustered data, which was a limitation of the project. If the WT M3 mouse did indeed have some neurodegenerative disease, possibly even a non-ApoE-induced form of AD, then its high degree of staining would lend additional credence to this project's conclusions. This would also explain why the male WT MGVs were significantly higher than the male ApoE3 MGVs despite both WT and ApoE3 being control groups and despite their similarity in the female data (**Fig. 12A, 13A**).

Interestingly, higher EB intensity was observed in females compared to males for ApoE4 and ApoE3 genotypes. WT mice did not exhibit any variation in BBB dysfunction across sex groups. Although the reason behind this difference due to sex is unclear, it could provide further evidence that females are at higher risk for AD and could suggest that this increased risk may be linked to the BBB and the *ApoE* gene itself, since both ε4 and ε3 mice displayed variance due to sex. How this data fit into the characterization of ApoE3 as a neutral variant is unknown, and further research is required to untangle this mystery. Additionally, a larger sample size of mice could reduce the impact of outliers on data and may find that no such difference exists.

*Limitations*

Some limitations were associated with this project, namely in the statistical analysis. The current statistical method does not properly address our data structure, as several slices originate from the same animal, producing clustered data. To properly take this into account, we would need to use an advanced method such as a generalized linear mixed-effect (GLME) model analysis. A

sample size of $n = 3$ animals per group is rather low and allows outliers and natural variation to impact the data significantly. Additionally, some more optimization of the slice preparation protocol would maximize retention of EB within the brain. EB from slices has the potential to escape into PBS when stored in well plates. Immediately transferring slices of interest to slides may address this challenge. Furthermore, the time in between slicing and mounting on slides was not standardized, and this may have affected the data, especially by allowing EB to leak into the PBS and result in either indiscriminate staining of entire slices or much darker slices. Once again, immediate transfer of slices to slides is a possible solution. Another is simply to standardize the storage time. To further decrease any variation in EB intensity caused by outside influences, using new petri dishes and brushes for each brain rather than for each group may ensure that all stains present in a slice originate from the same brain. Finally, as my skill at mounting slides improved over time, the amount of air bubbles present also decreased. These air bubbles have the potential to make images of slides blurry or trap pockets of EB dye. More slide mounting training time prior to beginning work on this thesis would have prevented this.

*Future Paths*

We have identified some promising paths for future research in addition to the suggestions mentioned in previous sections. An expanded version of this study could be conducted with a new independent variable of age, which would allow us to study the time-course of the BBB breakdown and its association with the progression of AD. This study would compare young, old, and middle-aged mice rather than simply focusing on the aged population we have chosen for this thesis. Another option for an expanded study would be to look at slides throughout the entirety, or at least vast chunks of, the brain, from the olfactory bulbs to the cerebellum. Because AD is a whole-brain disease, it is difficult to identify sections of the brain we can use as a control, but a whole-brain visualization would allow us to identify regions of diminished staining and limited BBB breakdown.

This method would nonetheless provide much more insights into key regions involved in and affected by AD and into the patterns of BBB breakdown than the comparatively limited investigation we have conducted in this thesis. Finally, this study identified the substantia nigra pars reticulata as a possibly significant but understudied (in relation to AD) region. Future studies may choose to further investigate whether this area does in fact contribute to or is involved in AD, especially in light of research implicating GABA and GABAergic neuron dysfunction in cognitive decline (Xu et al., 2020; Solas et al., 2015; Murari et al., 2020).

## References

Alzheimer's Association (2023). 2023 Alzheimer's disease facts and figures. Alzheimer's & Dementia *19*, 1598–1695. 10.1002/alz.13016.

Bell, R.D., Winkler, E.A., Singh, I., Sagare, A.P., Deane, R., Wu, Z., Holtzman, D.M., Betsholtz, C., Armulik, A., Sallstrom, J., et al. (2012). Apolipoprotein E controls cerebrovascular integrity via cyclophilin A. Nature *485*, 512–516. 10.1038/nature11087.

Cai, Z., Qiao, P.-F., Wan, C.-Q., Cai, M., Zhou, N.-K., and Li, Q. (2018). Role of Blood-Brain Barrier in Alzheimer's Disease. J Alzheimers Dis *63*, 1223–1234. 10.3233/JAD-180098.

Cummings, J.L. (2008). Update on Alzheimer's Disease: One Hundred Years After Dr. Alois Alzheimer. CNS Spectrums *13*, 4–6. 10.1017/S1092852900002819.

Deane, R., and Zlokovic, B.V. (2007). Role of the blood-brain barrier in the pathogenesis of Alzheimer's disease. Curr Alzheimer Res *4*, 191–197. 10.2174/156720507780362245.

Dickstein, D.L., Biron, K.E., Ujiie, M., Pfeifer, C.G., Jeffries, A.R., and Jefferies, W.A. (2006). Aβ peptide immunization restores blood-brain barrier integrity in Alzheimer disease. The FASEB Journal *20*, 426–433. 10.1096/fj.05-3956com.

Donahue, J.E., Flaherty, S.L., Johanson, C.E., Duncan, J.A., Silverberg, G.D., Miller, M.C., Tavares, R., Yang, W., Wu, Q., Sabo, E., et al. (2006). RAGE, LRP-1, and amyloid-beta protein in Alzheimer's disease. Acta Neuropathol *112*, 405–415. 10.1007/s00401-006-0115-3.

Erickson, M.A., and Banks, W.A. (2013). Blood–Brain Barrier Dysfunction as a Cause and Consequence of Alzheimer's Disease. J Cereb Blood Flow Metab *33*, 1500–1513. 10.1038/jcbfm.2013.135.

Fullerton, S.M., Shirman, G.A., Strittmatter, W.J., and Matthew, W.D. (2001). Impairment of the blood-nerve and blood-brain barriers in apolipoprotein e knockout mice. Exp Neurol *169*, 13–22. 10.1006/exnr.2001.7631.

Gauthier, S., Webster, C., Servaes, S., Morais, J., and Rosa-Neto, P. World Alzheimer Report 2022: Life after diagnosis: Navigating treatment, care and support. Alzheimer's Disease International.

Halliday, M.R., Rege, S.V., Ma, Q., Zhao, Z., Miller, C.A., Winkler, E.A., and Zlokovic, B.V. (2016). Accelerated pericyte degeneration and blood-brain barrier breakdown in apolipoprotein E4 carriers with Alzheimer's disease. J Cereb Blood Flow Metab *36*, 216–227. 10.1038/jcbfm.2015.44.

Hardy, J.A., and Higgins, G.A. (1992). Alzheimer's Disease: The Amyloid Cascade Hypothesis. Science *256*, 184–185.

Hawkins, B.T., and Egleton, R.D. (2006). Fluorescence imaging of blood–brain barrier disruption. Journal of Neuroscience Methods *151*, 262–267. 10.1016/j.jneumeth.2005.08.006.

Henstridge, C.M., Hyman, B.T., and Spires-Jones, T.L. (2019). Beyond the neuron-cellular interactions early in Alzheimer disease pathogenesis. Nat Rev Neurosci *20*, 94–108. 10.1038/s41583-018-0113-1.

Herrup, K. (2015). The case for rejecting the amyloid cascade hypothesis. Nat Neurosci *18*, 794–799. 10.1038/nn.4017.

Honeycutt, S.E., and O'Brien, L.L. (2021). Injection of Evans blue dye to fluorescently label and image intact vasculature. BioTechniques *70*, 181–185. 10.2144/btn-2020-0152.

Honig, L.S., Vellas, B., Woodward, M., Boada, M., Bullock, R., Borrie, M., Hager, K., Andreasen, N., Scarpini, E., Liu-Seifert, H., et al. (2018). Trial of Solanezumab for Mild Dementia Due to Alzheimer's Disease. New England Journal of Medicine *378*, 321–330. 10.1056/NEJMoa1705971.

Hultman, K., Strickland, S., and Norris, E.H. (2013). The APOE ε4/ε4 genotype potentiates vascular fibrin(ogen) deposition in amyloid-laden vessels in the brains of Alzheimer's disease patients. J Cereb Blood Flow Metab *33*, 1251–1258. 10.1038/jcbfm.2013.76.

Jackson, R.J., Meltzer, J.C., Nguyen, H., Commins, C., Bennett, R.E., Hudry, E., and Hyman, B.T. (2022). APOE4 derived from astrocytes leads to blood–brain barrier impairment. Brain *145*, 3582–3593. 10.1093/brain/awab478.

Kubotera, H., Ikeshima-Kataoka, H., Hatashita, Y., Allegra Mascaro, A.L., Pavone, F.S., and Inoue, T. (2019). Astrocytic endfeet re-cover blood vessels after removal by laser ablation. Sci Rep *9*, 1263. 10.1038/s41598-018-37419-4.

Lesné, S., Koh, M.T., Kotilinek, L., Kayed, R., Glabe, C.G., Yang, A., Gallagher, M., and Ashe, K.H. (2006). A specific amyloid-β protein assembly in the brain impairs memory. Nature *440*, 352–357. 10.1038/nature04533.

Li, W., Howard, J.D., and Gottfried, J.A. (2010). Disruption of odour quality coding in piriform cortex mediates olfactory deficits in Alzheimer's disease. Brain *133*, 2714–2726. 10.1093/brain/awq209.

Manaenko, A., Chen, H., Kammer, J., Zhang, J.H., and Tang, J. (2011). Comparison Evans Blue Injection Routes: Intravenous vs. Intraperitoneal, for Measurement of Blood-Brain Barrier in a Mice Hemorrhage Model. J Neurosci Methods *195*, 206–210. 10.1016/j.jneumeth.2010.12.013.

Márquez-Valadez, B., Rábano, A., and Llorens-Martín, M. (2022). Progression of Alzheimer's disease parallels unusual structural plasticity of human dentate granule cells. Acta Neuropathologica Communications *10*, 125. 10.1186/s40478-022-01431-7.

Mizuta, K. (2023). [Visualization of the functional neural circuit breakdown process in a mouse model of Alzheimer's disease and application to the development of new therapies]. Nihon Yakurigaku Zasshi *158*, 144–149. 10.1254/fpj.22119.

Montagne, A., Nation, D.A., Sagare, A.P., Barisano, G., Sweeney, M.D., Chakhoyan, A., Pachicano, M., Joe, E., Nelson, A.R., D'Orazio, L.M., et al. (2020). APOE4 leads to blood–brain barrier dysfunction predicting cognitive decline. Nature *581*, 71–76. 10.1038/s41586-020-2247-3.

Muldoon, L.L., Pagel, M.A., Kroll, R.A., Roman-Goldstein, S., Jones, R.S., and Neuwelt, E.A. (1999). A physiological barrier distal to the anatomic blood-brain barrier in a model of transvascular delivery. AJNR Am J Neuroradiol *20*, 217–222.

Murari, G., Liang, D.R.-S., Ali, A., Chan, F., Mulder-Heijstra, M., Verhoeff, N.P.L.G., Herrmann, N., Chen, J.J., and Mah, L. (2020). Prefrontal GABA Levels Correlate with Memory in Older Adults at High Risk for Alzheimer's Disease. Cerebral Cortex Communications *1*, tgaa022. 10.1093/texcom/tgaa022.

Murphy, C. (2019). Olfactory and other sensory impairments in Alzheimer disease. Nat Rev Neurol *15*, 11–24. 10.1038/s41582-018-0097-5.

National Institute on Aging (2023). Alzheimer's Disease Genetics Fact Sheet. National Institute on Aging. https://www.nia.nih.gov/health/alzheimers-disease-genetics-fact-sheet.

Ohm, T.G. (2007). The dentate gyrus in Alzheimer's disease. Prog Brain Res *163*, 723–740. 10.1016/S0079-6123(07)63039-8.

Oishi, K., and Lyketsos, C.G. (2014). Alzheimer's disease and the fornix. Frontiers in Aging Neuroscience *6*.

Orta-Salazar, E., Feria-Velasco, A.I., and Díaz-Cintra, S. (2019). Primary motor cortex alterations in Alzheimer disease: a study in the 3xTg-AD model. Neurología (English Edition) *34*, 429–436. 10.1016/j.nrleng.2019.02.001.

Pardilla-Delgado, E., Torrico-Teave, H., Sanchez, J.S., Ramirez-Gomez, L.A., Baena, A., Bocanegra, Y., Vila-Castelar, C., Fox-Fuller, J.T., Guzmán-Vélez, E., Martínez, J., et al. (2021). Associations between subregional thalamic volume and brain pathology in autosomal dominant Alzheimer's disease. Brain Commun *3*, fcab101. 10.1093/braincomms/fcab101.

Piller, C. (2022). Blots on a Field? Potential fabrication in research images threatens key theory of Alzheimer's disease. Science. https://www.science.org/content/article/potential-fabrication-research-images-threatens-key-theory-alzheimers-disease.

Ray, B., and Keyrouz, S.G. (2014). Management of anticoagulant-related intracranial hemorrhage: an evidence-based review. Crit Care *18*, 223. 10.1186/cc13889.

Richetin, K., Steullet, P., Pachoud, M., Perbet, R., Parietti, E., Maheswaran, M., Eddarkaoui, S., Bégard, S., Pythoud, C., Rey, M., et al. (2020). Tau accumulation in astrocytes of the dentate gyrus induces neuronal dysfunction and memory deficits in Alzheimer's disease. Nat Neurosci *23*, 1567–1579. 10.1038/s41593-020-00728-x.

Ríos, A.S., Oxenford, S., Neudorfer, C., Butenko, K., Li, N., Rajamani, N., Boutet, A., Elias, G.J.B., Germann, J., Loh, A., et al. (2022). Optimal deep brain stimulation sites and networks for stimulation of the fornix in Alzheimer's disease. Nat Commun *13*, 7707. 10.1038/s41467-022-34510-3.

Riphagen, J.M., Ramakers, I.H.G.M., Freeze, W.M., Pagen, L.H.G., Hanseeuw, B.J., Verbeek, M.M., Verhey, F.R.J., and Jacobs, H.I.L. (2020). Linking APOE-ε4, blood-brain barrier dysfunction, and

inflammation to Alzheimer's pathology. Neurobiology of Aging *85*, 96–103. 10.1016/j.neurobiolaging.2019.09.020.

Saiz-Sanchez, D., De la Rosa-Prieto, C., Ubeda-Banon, I., and Martinez-Marcos, A. (2015). Interneurons, tau and amyloid-β in the piriform cortex in Alzheimer's disease. Brain Struct Funct *220*, 2011–2025. 10.1007/s00429-014-0771-3.

Salloway, S., Gur, T., Berzin, T., Tavares, R., Zipser, B., Correia, S., Hovanesian, V., Fallon, J., Kuo-Leblanc, V., Glass, D., et al. (2002). Effect of APOE genotype on microvascular basement membrane in Alzheimer's disease. J Neurol Sci *203–204*, 183–187. 10.1016/s0022-510x(02)00288-5.

Segarra, M., Aburto, M.R., and Acker-Palmer, A. (2021). Blood–Brain Barrier Dynamics to Maintain Brain Homeostasis. Trends in Neurosciences *44*, 393–405. 10.1016/j.tins.2020.12.002.

Sharma, H.S., and Ali, S.F. (2008). Acute Administration of 3,4-Methylenedioxymethamphetamine Induces Profound Hyperthermia, Blood–Brain Barrier Disruption, Brain Edema Formation, and Cell Injury. Annals of the New York Academy of Sciences *1139*, 242–258. 10.1196/annals.1432.052.

Shen, Y., Zhang, A., Guo, J., Dan, G., Chen, S., and Yu, H. (2014). Fluorescence imaging of Evans blue extravasation into mouse brain induced by low frequency ultrasound with microbubble. Bio-Medical Materials and Engineering *24*, 2831–2838. 10.3233/BME-141101.

Solas, M., Puerta, E., and Ramirez, M.J. (2015). Treatment Options in Alzheimer´s Disease: The GABA Story. Curr Pharm Des *21*, 4960–4971. 10.2174/1381612821666150914121149.

Suvà, D., Favre, I., Kraftsik, R., Esteban, M., Lobrinus, A., and Miklossy, J. (1999). Primary motor cortex involvement in Alzheimer disease. J Neuropathol Exp Neurol *58*, 1125–1134. 10.1097/00005072-199911000-00002.

Sweeney, M.D., Sagare, A.P., and Zlokovic, B.V. (2018). Blood–brain barrier breakdown in Alzheimer disease and other neurodegenerative disorders. Nat Rev Neurol *14*, 133–150. 10.1038/nrneurol.2017.188.

Takamura, R., Mizuta, K., Sekine, Y., Islam, T., Saito, T., Sato, M., Ohkura, M., Nakai, J., Ohshima, T., Saido, T.C., et al. (2021). Modality-Specific Impairment of Hippocampal CA1 Neurons of Alzheimer's Disease Model Mice. J Neurosci *41*, 5315–5329. 10.1523/JNEUROSCI.0208-21.2021.

Teleanu, R.I., Preda, M.D., Niculescu, A.-G., Vladâcenco, O., Radu, C.I., Grumezescu, A.M., and Teleanu, D.M. (2022). Current Strategies to Enhance Delivery of Drugs across the Blood–Brain Barrier. Pharmaceutics *14*, 987. 10.3390/pharmaceutics14050987.

Thal, D.R., Holzer, M., Rüb, U., Waldmann, G., Günzel, S., Zedlick, D., and Schober, R. (2000). Alzheimer-Related τ-Pathology in the Perforant Path Target Zone and in the Hippocampal Stratum Oriens and Radiatum Correlates with Onset and Degree of Dementia. Experimental Neurology *163*, 98–110. 10.1006/exnr.2000.7380.

Wang, H.-L., Kuo, E.Y., and Lai, T.W. (2018). Vascular delivery of intraperitoneal Evans blue dye into the blood-brain barrier-intact and disrupted rat brains. Neuroreport *29*, 924–931. 10.1097/WNR.0000000000001052.

Wang, H.-L., and Lai, T.W. (2014). Optimization of Evans blue quantitation in limited rat tissue samples. Sci Rep *4*, 6588. 10.1038/srep06588.

Wang, Y., Liu, J., Zhang, Z., Wang, X., and Zhang, C. (2011). Structure and permeability changes of the blood-brain barrier in APP/PS1 mice: an Alzheimer's disease animal model. Neurochem. J. *5*, 220–222. 10.1134/S1819712411030135.

Wessels, A.M., Lines, C., Stern, R.A., Kost, J., Voss, T., Mozley, L.H., Furtek, C., Mukai, Y., Aisen, P.S., Cummings, J.L., et al. (2020). Cognitive outcomes in trials of two BACE inhibitors in Alzheimer's disease. Alzheimer's & Dementia *16*, 1483–1492. 10.1002/alz.12164.

Wiesman, A.I., Mundorf, V.M., Casagrande, C.C., Wolfson, S.L., Johnson, C.M., May, P.E., Murman, D.L., and Wilson, T.W. (2021). Somatosensory dysfunction is masked by variable cognitive deficits across patients on the Alzheimer's disease spectrum. EBioMedicine *73*, 103638. 10.1016/j.ebiom.2021.103638.

Yen, L.F., Wei, V.C., Kuo, E.Y., and Lai, T.W. (2013). Distinct Patterns of Cerebral Extravasation by Evans Blue and Sodium Fluorescein in Rats. PLoS One *8*, e68595. 10.1371/journal.pone.0068595.

Zenaro, E., Piacentino, G., and Constantin, G. (2017). The blood-brain barrier in Alzheimer's disease. Neurobiology of Disease *107*, 41–56. 10.1016/j.nbd.2016.07.007.